nanomaterials

MDPI

Review

Recent Progress in Metal–Organic Framework (MOF) Based Luminescent Chemodosimeters

Yuanqiang Hao [1], Shu Chen [2], Yanli Zhou [1,*], Yintang Zhang [1] and Maotian Xu [1,3,*]

[1] Henan Key Laboratory of Biomolecular Recognition and Sensing, College of Chemistry and Chemical Engineering, Shangqiu Normal University, Shangqiu 476000, China
[2] Key Laboratory of Theoretical Organic Chemistry and Function Molecule of Ministry of Education, School of Chemistry and Chemical Engineering, Hunan University of Science and Technology, Xiangtan 411201, China
[3] College of Chemistry and Molecular Engineering, Zhengzhou University, Zhengzhou 450001, China
* Correspondence: zhouyanli@mails.ucas.ac.cn (Y.Z.); xumaotian@sqnu.edu.cn (M.X.); Tel.: +86-0370-3112844 (Y.Z.)

Received: 16 May 2019; Accepted: 17 June 2019; Published: 3 July 2019

Abstract: Metal–organic frameworks (MOFs), as a class of crystalline hybrid architectures, consist of metal ions and organic ligands and have displayed great potential in luminescent sensing applications due to their tunable structures and unique photophysical properties. Until now, many studies have been reported on the development of MOF-based luminescent sensors, which can be classified into two major categories: MOF chemosensors based on reversible host–guest interactions and MOF chemodosimeters based on the irreversible reactions between targets with a probe. In this review, we summarize the recently developed luminescent MOF-based chemodosimeters for various analytes, including H_2S, HClO, biothiols, fluoride ions, redox-active biomolecules, Hg^{2+}, and CN^-. In addition, some remaining challenges and future perspectives in this area are also discussed.

Keywords: metal–organic frameworks; luminescent sensor; chemodosimeter; review

1. Introduction

Metal–organic frameworks (MOFs), constructed by metal ions (or clusters) with organic ligands, are a subclass of coordination polymers with highly crystalline structures [1,2]. In the past two decades, enormous progress has been made in the synthesis and application of MOFs [3–5]. Because of their remarkable structural features, such as high porosity and large surface area, as well as their exceptional physicochemical properties, MOFs possess versatile applications in gas storage and separation [6–11], heterogeneous catalysis [12–15], drug delivery and chemotherapy [16,17], and sensing [18,19]. As new types of promising functional materials, luminescent MOFs especially have great potential as alternative phosphors in lighting devices and luminescent sensors [20–23].

Due to the versatile building blocks of MOFs (inorganic ions and organic ligand molecules), as well as their structural diversity, the photoluminescence of MOFs can arise from a variety of possibilities [20]: (i) luminescence from organic linkers, which are normally extended π-conjugation systems with rigid structures, such as pyrene, anthracene, and their derivatives; (ii) metal-based emissions, e.g., MOFs with metal centers of lanthanoid; (iii) a metal–to–ligand charge transfer (MLCT), e.g., d^{10} Cu(I)- and Ag(I)-based MOFs; (iv) a ligand–to–metal charge transfer (LMCT), e.g., Zn(II)/Cd(II) and carboxylate ligand based MOFs; (v) antennae effects; and (vi) sensitization, e.g., MOFs with absorbing ligands and emitting lanthanoid ions (Figure 1). In the past, the competent luminescence features of MOFs have been extensively studied and exploited in fluorescence imaging and sensing applications [24]. These developed MOF-based luminescent probes can be classified into two types according to the recognition mechanism between the probe with the target analyte: (1) an MOF-based chemosensor,

in which the analyte coordinates or interacts with the probe in a reversible manner, such as via physical/electrostatic interaction; (2) an MOF-based chemodosimeter, in which the target analyte can irreversibly react with a probe to yield a product that is chemically different from the starting probe via target-induced oxidation, hydrolysis, and nucleophilic processes.

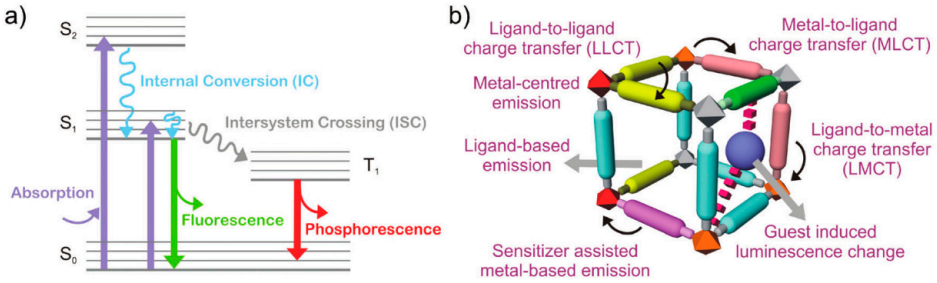

Figure 1. (**a**) Partial energy-level diagram for photoluminescent processes; (**b**) various possibilities for the emission of metal–organic frameworks (MOFs). Reproduced with permission from [24]. Copyright the Royal Society of Chemistry, 2017.

MOF-based luminescent chemosensors have shown great potential in the detection of various analytes, including volatile organic compounds [25–27], ions (especially for metal cations) [28–31], gases [32–35], as well as for monitoring pH [36–42], humidity [43–45], and temperature [46–48]. Compared to the relatively well-developed fluorescent MOFs chemosensors, MOF-based chemodosimeters are expected to be more efficient in terms of selectivity, as they exploit the specific reactivities of certain target analytes [24]. Moreover, numerous MOF-based luminescent chemodosimeters can be afforded by introducing various recognition moieties for different analytes into building blocks. In the past several years, considerable effort has been expended in this field, and research interest is still growing. In spite of this interest, to date, the studies concerning MOF-based chemodosimeters have not yet been comprehensively addressed. To fill this gap, in the present review, we will make an effort to summarize recent progress in the development of MOF-based chemodosimeters. Moreover, the promising prospects and remaining challenges for future research in the field will also be discussed.

2. MOF-Based Luminescent Chemodosimeters for Sulfur Compounds

2.1. MOF-Based Chemodosimeters for H_2S

Hydrogen sulfide (H_2S), the smallest sulfhydryl compound, exists as a typical rotten egg smelling gas in the air or as a hydrosulfide ion while being dissolved in an aqueous solution under neutral pH conditions. Traditionally, H_2S was simply considered to be an environmentally toxic species. In recent years, H_2S has been discovered to be an essential biological molecule that can function as a cytoprotectant and gasotransmitter in organisms [49,50]. Moreover, the metabolism of H_2S is closely related to various physiological and pathological events in the human body [51,52]. In this context, the development of new methods for sensing H_2S and studying its biological roles has attracted tremendous attention [53–55]. Fluorescence technology is particularly promising for such purposes, as it enables monitoring of the target with superior temporal and spatial resolution [56–59], especially for in vivo applications. By exploiting its unique characteristics, such as strong nucleophilicity and ability to reduce potency, various small-molecule fluorescent probes have been developed for detecting and imaging H_2S. These probes can be mainly categorized into three types according to their sensing strategy: (i) sensors based on the H_2S-mediated reduction of an azide/nitro group to the amine [60–63]; (ii) sensors based on the H_2S-participated nucleophilic reaction [64–67]; and (iii) sensors based on the binding reaction between sulfide and Cu^{2+} [68,69]. By exploiting the similar sensing strategies and carefully employing post-synthetic modification approaches, a number of MOF-based fluorescent H_2S probes (Table 1) were successfully constructed in the last few years [70].

Table 1. List of MOF-based luminescent chemodosimeters for H_2S.

MOF Formula	$\lambda_{ex}/\lambda_{em}$ (nm)	Dynamic Range	LOD [1]	RT [2]	Media	Real Sampe	Ref.
$Zr_6O_4(OH)_4(BDC\text{-}N_3)_6$	334/436	0–4 mM	117 μM	180 s	HEPES buffer (10 mM, pH 7.4)	Live cells	[71]
$Zr_6O_4(OH)_4(BDC\text{-}NO_2)_6$	334/436	0–4 mM	188 μM	460 s	HEPES buffer (10 mM, pH 7.4)	–	[72]
$Zn_4O(OH)_4(BDC\text{-}N_3)_3$	395/455	0–0.5 mM	28.3 μM	90 s	HEPES ethanol buffer (10 mM, pH 7.4)	–	[73]
$Ce_6O_4(OH)_4(BDC\text{-}N_3)_6$	334/429	0–3.5 mM	12.2 μM	760 s	HEPES buffer (10 mM, pH 7.4)	–	[74]
$Ce_6O_4(OH)_4(BDC\text{-}NO_2)_6$	334/429	0–3.5 mM	34.8 μM	480 s	HEPES buffer (10 mM, pH 7.4)	–	[74]
$Al(OH)(IPA\text{-}N_3)$	330/405	0–0.06 mM	2.65 μM	420 s	HEPES buffer (10 mM, pH 7.4)	Live cells	[75]
$Zr_6O_4(OH)_4((NDC\text{-}(NO_2)_2)_6$	390/474	0.1–0.7 mM	20 μM	50 min	HEPES buffer (10 mM, pH 7.4)	Live cells	[76]
$Al(OH)(BDC\text{-}N_3)$	315/425	0.2–1.6 μM	90.47 nM	60 s	HEPES buffer (10 mM, pH 7.4)	Live cells	[77]
$Al_3O_4(OH)_4(BDC\text{-}(NO_2)_2)_6$	345/527	0.1–0.6 mM	14.14 μM	40 min	HEPES buffer (10 mM, pH 7.4)	Live cells	[78]
$Al_3(O)(OH)(BDC\text{-}N_3)_3$	343/460, 565	0.1–120 μM	100 nM	–	Hank's balanced salt solution	Cell sample	[79]
$Al(OH)(BDC\text{-}NO_2)$/poly(vinylidene fluoride)	396/466	0–0.1 mM	92.31 nM	–	PVDF membrane	Lake water	[80]
$Cu(TCPP)[AlOH]_2$	419/602, 650	0–10 μM	16 nM	instant	BBS buffer (20 mM, pH 7.4)	Live cells	[81]
CuO@TO@UiO-66	510/~560	0–100 μM	0.51 μM	instant	Tris-HCl butter (20 mM, pH 7.4)	Live cells	[82]
Eu^{3+}/Cu^{2+}@UiO-66-$(COOH)_2$	305/393, 615	0–625 μM	5.45 μM	30 s	HEPES buffer (10 mM, pH 7.4)	–	[83]
Eu^{3+}/Ag^{+}@UiO-66-$(COOH)_2$	305/615	0–2.5 mM	23.53 μM	30 s	HEPES buffer (10 mM, pH 7.4)	Serum	[84]
Tb^{3+}@$[Cu(CPOC)_2]$	280/390, 544	0–1.6 mM	13.25 μM	2 min	HEPES buffer (10 mM, pH 7.4)	–	[85]
UiO-66-CH = CH_2 $Zr_6O_4(OH)_4(BDC\text{-}CH = CH_2)_6$	328/382	0–0.05 mM	6.46 μM	10 s	HEPES buffer (10 mM, pH 7.4)	Live cells	[86]
Fe^{III}-MIL-88-NH_2	333/~440	60–100 μM	10 μM	5 min	Aqueous solution	–	[87]

[1] LOD means limit of detection. [2] RT means reaction time.

2.1.1. Based on the H_2S-Mediated Reduction of Azide/Nitro Group to Amine

Ghosh et al. first reported a Zr-based MOF, $Zr_6O_4(OH)_4(BDC\text{-}N_3)_6$ (UiO-66@N_3), bearing an azide group for sensing H_2S [71]. The MOF-based chemodosimeter UiO-66@N_3 was prepared via post modification of the amine functionalized UiO-66@NH_2 using an azidation agent. UiO-66@N_3 is highly stable in an aqueous solution and fluoresces very weakly due to the presence of an electron-deficient azide group (Figure 2). Treating UiO-66@N_3 with Na_2S in an HEPES (4-(2-hydroxyethyl)-1-piperazineethanesulfonic acid) aqueous buffer (10 mM, pH 7.4) creates a strong emission (16-fold enhancement), which can be ascribed to the target-mediated reduction of azide to amine, which produces the luminescent UiO-66@NH_2. This conversion process is characterized by FTIR (Fourier Transform infrared spectroscopy) and NMR (Nuclear Magnetic Resonance Spectroscopy) studies. UiO-66@N_3 can respond rapidly to H_2S (less than 180 s) with high selectivity over other interferences, including most abundant biothiols (Cys and GSH). Moreover, UiO-66@N_3 also displays low cell viability and has been applied to live cell imaging studies. The same research group subsequently prepared a nitro-functionalized Zr-MOF (UiO-66@NO_2) for the fluorescence turn-on detection of H_2S, in which UiO-66@NO_2 can be facilely obtained in a single synthetic step by using 2-nitroterephthalic acid as the ligand [72]. Incorporation of the azide/nitro group onto other MOFs scaffolds has afforded a variety of luminescent H_2S chemodosimeters. Qian et al. reported an azide-appended Zn-MOF for the fluorescent turn-on detection of H_2S [73]. In a HEPES ethanol buffer, the probe displayed excellent selectivity and a rapid response time for H_2S. By directly reacting the cerium(IV) nitrate with an azide/nitro-substituted 1,4-benzenedicarboxylate (BDC), Biswas et al. synthesized two Ce-MOFs (Ce-UiO-66@N_3, Ce-UiO-66@NO_2) for sensing H_2S [74]. Since then, the Biswas group has developed a number of reaction-based luminescent H_2S sensors, including Al(OH)(IPA-N_3) [75], $Zr_6O_4(OH)_4$((NDC-$(NO_2)_2)_6$ [76], Al(OH)(BDC-N_3) [77], and $Zr_6O_4(OH)_4$(BDC-$(NO_2)_2)_6$ [78]. Further, Al(OH)(BDC-N_3) was also employed as a turn-off fluorimetric sensor for detecting Fe(III) in an aqueous solution [77].

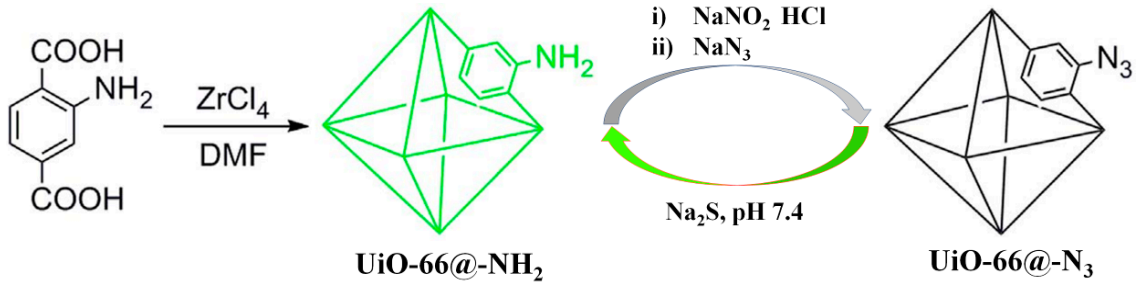

Figure 2. The synthetic route and sensing mechanism of UiO-66@N_3 for H_2S. Reproduced with permission from [71]. Copyright Nature Publishing Group, 2014.

Canivet et al. reported an Al-MOF, $Al_3(O)(OH)(BDC\text{-}N_3)_3$ (Al-MIL-101-N_3, Figure 3a) based sensing system for H_2S [79]. It is worth noting that the use of a femtosecond (fs)-pulse laser excitation can significantly improve the emission features as well as the analytical performances of this MOF-based luminescent assay. All these investigated BDC-based MOFs (Al-MIL-101-NH_2, In-MIL-68-NH_2, and Zr-UiO-66-NH_2) displayed characteristic emissions at about 460 nm (Figure 3b) under UV-lamp excitation at 343 nm. While under fs-pulse laser excitation, Al-MIL-101-NH_2 revealed another predominent emission band centered at 565 nm, which may have resulted from an increase of the luminescence center in the electronic excited state and the redistribution of the photoexcited charge carriers (Figure 3c,d). The spectral behaviors of Al-MIL-101-N_3 for H_2S were studied in DMSO (dimethyl sulfoxide) as well as in HBSS (Hank's balanced salt solution). In the biological media of HBSS, Al-MIL-101-N_3 displayed a wide dynamic range of 0.1–120 μM and a low LOD of 100 nM for H_2S (Figure 3e,f). Moreover, Al-MIL-101-N_3 was applied to detect sulfide from an exogenous small molecule releaser (GYY4137) and endogenous H_2S produced by 3T3L1 cells (Figure 3g,h).

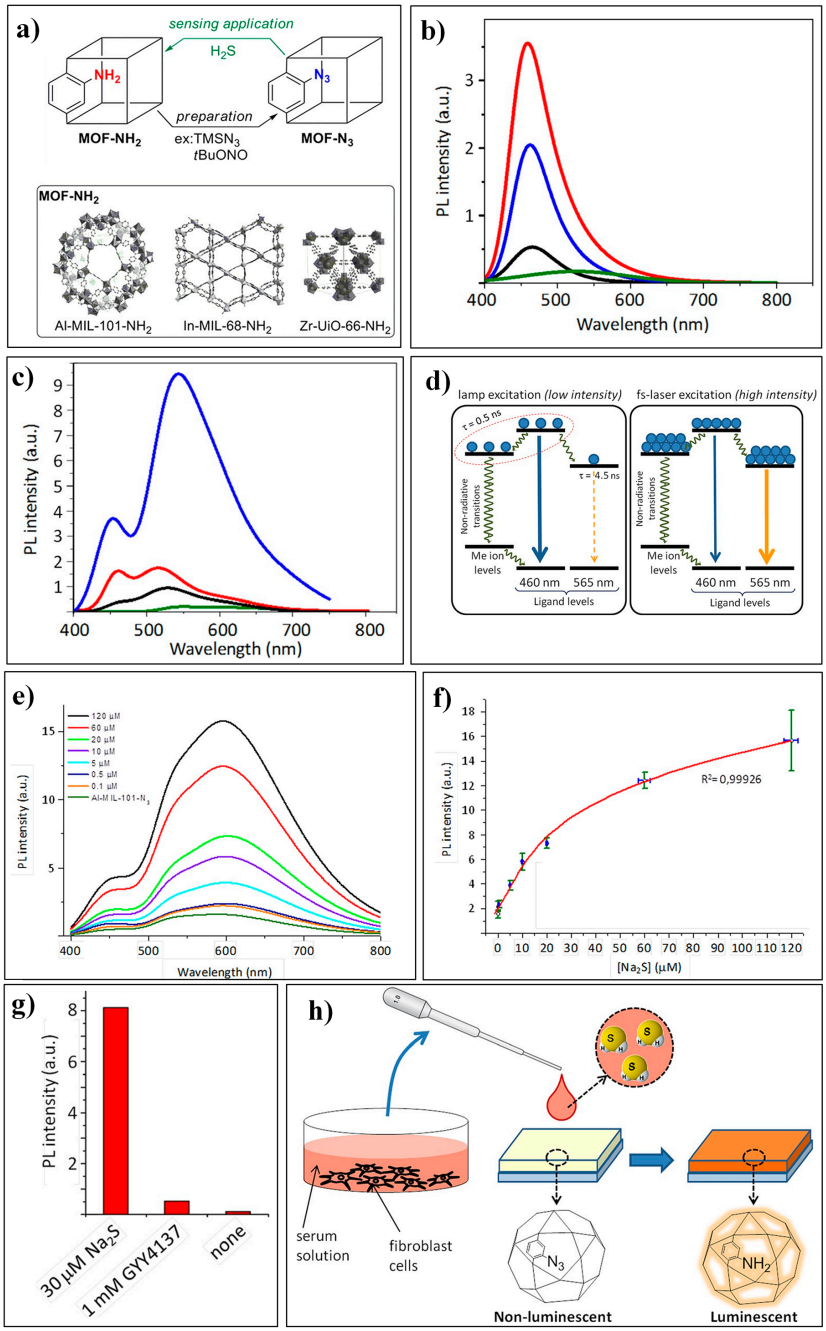

Figure 3. (**a**) Azido-MOFs for H_2S sensing. (**b**,**c**) Emission spectra of dry MOF samples, Al-MIL-101-NH_2 (blue), In-MIL-68-NH_2 (red), Zr-UiO-66-NH_2 (black), Al-MIL-101-N_3 (green) under UV-lamp excitation (**b**) or fs-pulse laser excitation (**c**) at 343 nm. (**d**) Proposed schematic mechanisms of charges recombination underpinning the observed switch in emission channels. (**e**) Emission spectra of Al-MIL-101-N_3 in the presence of different concentrations of sodium sulfide (excited at 343 nm with a fs-pulse laser). (**f**) Reversed cubic fit of sodium sulfide concentration vs. measured intensity of the 565 nm band in emission spectra. (**g**) Detection of H_2S released from GYY4137. (**h**) Exposure of Al-MIL-101-N_3 to a sample of culture medium for cells with endogenously produced H_2S. Reproduced with permission from [79]. Copyright Wiley-VCH, 2016.

By integrating Al-MOF (Al(OH)(BDC-NO_2), Al-MIL-53-NO_2), and poly(vinylidene fluoride) (PVDF), Qian et al. developed a novel MMM (MOF-polymer mixed-matrix membrane) for the fluorescence turn-on detection of H_2S [80]. The Al-MIL-53-NO_2@PVDF MMM can be readily prepared with a high loading of the MOF probes (70 wt%), following the procedures as depicted in Figure 4a.

The obtained Al-MIL-53-NO_2 MMM is mechanically robust and flexible and can be easily handled. The Al-MIL-53-NO_2 MMM can be effectively applied to the flow-through detection of H_2S, which exhibited remarkably high sensitivity with an LOD of 92.31 nM (Figure 4b,c).

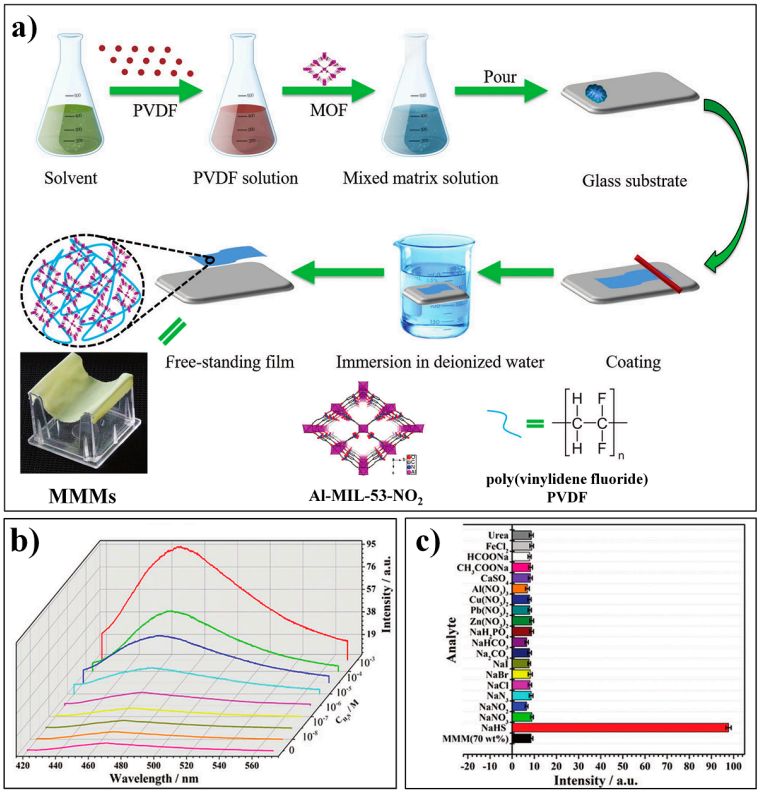

Figure 4. (**a**) Fabrication process for Al-MIL-53-NO_2@PVDF MOF-polymer mixed-matrix membranes (MMMs). (**b**) Fluorescence spectra of Al-MIL-53-NO_2@PVDF MMMs (70 wt%) with different concentrations of H_2S (excited at 396 nm). (**c**) Fluorescence response of Al-MIL-53-NO_2 MMMs at 466 nm toward various analytes. Reproduced with permission from [80]. Copyright Wiley-VCH, 2016.

Furthermore, the constructed Al-MIL-53-NO_2 MMM was also used to detect H_2S in real water samples.

2.1.2. Based on the Binding Reaction between S^{2-} and Cu^{2+}

Tang et al. firstly reported a Cu(II)-metalated MOF, Cu(TCPP)[AlOH]$_2$ (TCPP: *meso*-tetrakis(4-carboxylphenyl)porphyrin), for luminescent sensing of H_2S [81]. Cu(TCPP)[AlOH]$_2$ was obtained via Cu(II) metalation of the porphyrin ring-contained parent MOF TCPP[AlOH]$_2$(DMF)$_3$(H_2O)$_2$. The paramagnetic Cu(II) ions can quench the ligand-based (porphyrin) fluorescence of Cu(TCPP)[AlOH]$_2$. Upon the addition of H_2S, the Cu(II) ion can be taken from the porphyrin center via the formation of a CuS precipitate, thereby leading to the recovery of porphyrin-based emissions in the MOF system (Figure 5a). The fluorescence response of Cu(TCPP)[AlOH]$_2$ to H_2S can occur instantaneously with high sensitivity (LOD: 16 nM) and excellent selectivity as other analytes did not generate any fluorescence enhancement. Luminescence imaging studies also demonstrated that Cu(TCPP)[AlOH]$_2$ can be employed for monitoring both exogenous and endogenic H_2S in liver hepatocellular (HepG2) cells (Figure 5b). The Tang group recently developed a CuO NPs functionalized NMOF (Nanoscale metal–organic frameworks) hybrid nanoprobe, CuO@TO@UiO-66, for the sensing and imaging of H_2S [82]. Due to the energy transfer process from TO@UiO-66 to CuO NPs, the nanoprobe is weakly emissive. Sulfide can react with CuO to release the luminescent TO@UiO-66, thereby achieving a sensitive turn-on fluorescence response to H_2S.

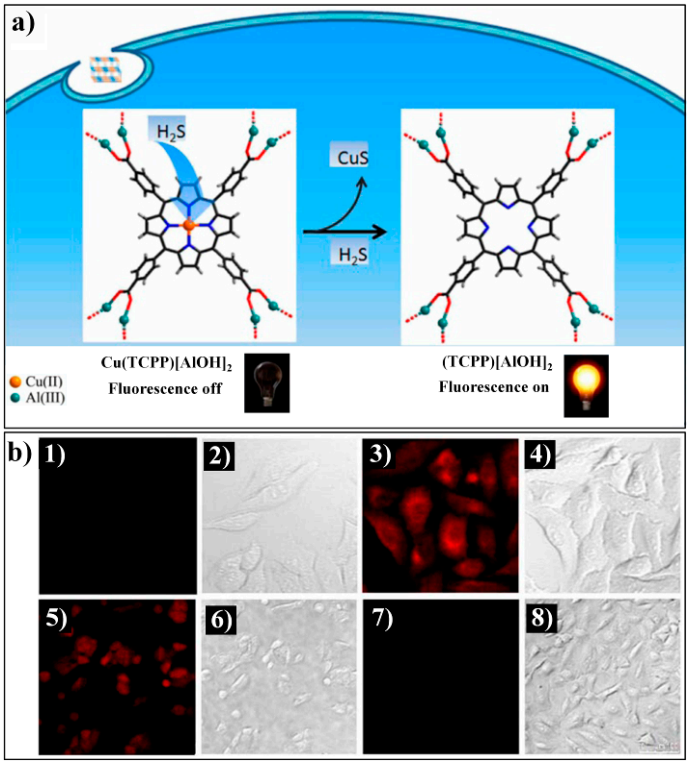

Figure 5. (**a**) The proposed strategy for the fluorescent variation of Cu(TCPP)[AlOH]$_2$ for H_2S. (**b**) Confocal fluorescence images in living cells: (1) image of HepG2 cells incubated with 10 μM Cu(TCPP)[AlOH]$_2$; (2) bright-field image of (1); (3) image of HepG2 cells incubated with 10 μM Cu(TCPP)[AlOH]$_2$ and 50 μM NaHS; (4) bright-field image of (3); (5) image of A549 cells incubated with 500 μM SNP and 10 μM Cu(TCPP)[AlOH]$_2$; (6) bright-field image of (5); (7) image of A549 cells incubated with 250 mg·L^{-1} DL-propargylglycine (PPG) and 10 μM Cu(TCPP)[AlOH]$_2$; (8) bright-field image of (7). Reproduced with permission from [81]. Copyright American Chemical Society, 2014.

Qian et al. prepared a nano MOF Eu^{3+}/Cu^{2+}@UiO-66-$(COOH)_2$ system for the ratiometric luminescent sensing of H_2S by the post-modification of UiO-66-$(COOH)_2$ with Eu^{3+} and Cu^{2+} ions [83]. This MOF system displayed two distinct emissions, a sharp Eu^{3+} emission at 615 nm and a broad ligand-based emission at 393 nm. Due to the decreased antenna efficiency of the H_4btec ligands to Eu^{3+} in the presence of Cu^{2+}, Eu^{3+}/Cu^{2+}@UiO-66-$(COOH)_2$ exhibited a weak Eu^{3+} emission and a relatively enhanced ligand-based emission. While the target sulfide can effectively snatch the copper ion from the MOF probe and result in a significant enhancement in the fluorescence intensity ratio (I_{615}/I_{393}), thus achieving a ratiometric fluorescence response for H_2S (Figure 6). Other advantageous features of this MOF sensor include excellent compatibility with aqueous media and instant response. However, it should be noted that other sulfhydryl compounds (i.e., GSH, Hcy, and Cys) also generated a certain degree of fluorescence response, which may be ascribed to the moderate binding affinity of H4btec to Cu^{2+}, and these interferences also competitively bind to Cu^{2+}. The same research group consequently developed a fluorescent MOF-based logic platform Eu^{3+}/Ag^{+}@UiO-66-$(COOH)_2$ for H_2S detection [84].

Yang et al. reported a luminescent composite Tb^{3+}@Cu-MOF for the turn-on ratiometric sensing of H_2S [85]. The synthesis process for Tb^{3+}@Cu-MOF and the sensing mechanism for H_2S are shown in Figure 7a. The Cu-MOF, [Cu(CPOC)$_2$] was firstly prepared by reacting copper salt with an organic ligand (CPOC: 5-(4′-carboxyphenoxy) nicotinic acid). SC-XRD (single crystal X-ray diffraction) analysis indicated that [Cu(CPOC)$_2$] belongs to the monoclinic system ($P2_1/c$), with a half crystallographically independent metal center and one ligand per asymmetric unit (Figure 7b). The probe Tb^{3+}@Cu-MOF can be readily obtained via post-grafting modification with Tb^{3+}. [Cu(CPOC)$_2$] displayed an emission

band at about 390 nm. Tb^{3+}@Cu-MOF showed additional emissions of the Tb^{3+} ion (at 489, 544, 585, and 620 nm) but with relatively weak intensities because the Cu^{2+} with an unsaturated electronic state ($3d^9$) has a tendency to gain electrons and thus quench the fluorescence. With the addtion of sulfide, Cu^{2+} can be bounded and, as a consequence its quenching effect, can be hindered, leading to a significant and selective increase in the characteristic emissions of Tb^{3+} (Figure 7c). Noticeably, the Tb^{3+}@Cu-MOF well retained its crystalline structure after being incubated with Na_2S.

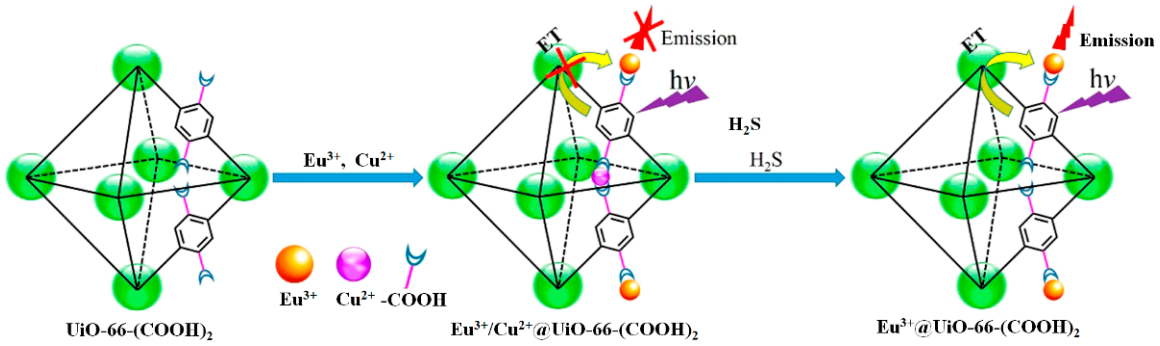

Figure 6. The fluorescence detection mechanism of the MOF Eu^{3+}/Cu^{2+}@UiO-66-$(COOH)_2$ system for H_2S. Reproduced with permission from [83]. Copyright American Chemical Society, 2016.

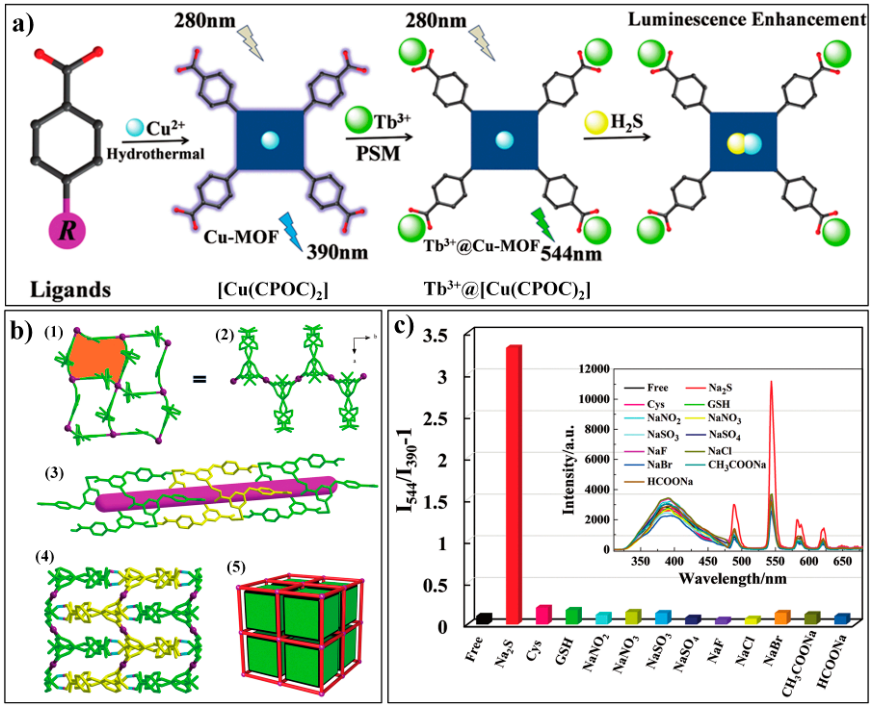

Figure 7. (**a**) Synthetic route for Tb^{3+}@Cu-MOF and its sensing mechanism for H_2S. (**b**) Crystalline structure of $[Cu(CPOC)_2]$, (1) 2D layers of Cu1; (2) 2D layers of Cu1 viewed along the c axis; (3) 1D channel in the 3D framework; (4) 3D supramolecular framework of $[Cu(CPOC)_2]$ through O–H···O interactions; (5) topological representation of the 3D structure. (**c**) Fluorescence response of Tb^{3+}@$[Cu(CPOC)_2]$ towards sulfide and other analytes. Reproduced with permission from [85]. Copyright the Royal Society of Chemistry, 2017.

2.1.3. Other MOF-Based Chemodosimeters for H_2S

Cui et al. designed a vinyl-functionalized Zr-MOF (UiO-66-CH = CH_2) for detecting H_2S by using 2-vinylterephthalic acid as the linker ligand [86]. UiO-66-CH = CH_2 showed a turn-off fluorescence response toward H_2S with high sensitivity and selectivity. This probe also featured low toxicity and

good water stability, but the sensing mechanism is not discussed in this study. Wang et al. reported a novel turn-on fluorescent assay for H_2S based on the target-mediated collapse of an MOF structure ($Fe_3O(OH_2)_3(BDC\text{-}NH_2)_3$, Fe^{III}-MIL-88-NH_2) (Figure 8) [87]. Due to the paramagnetic nature of Fe(III), Fe^{III}-MIL-88-NH_2 is non-emissive. Mixing the Fe^{III}-MIL-88-NH_2 suspension with a NaHS solution can lead to the breakdown of the MOFs and a release of the luminescent ligand of 2-aminoterephthalic acid.

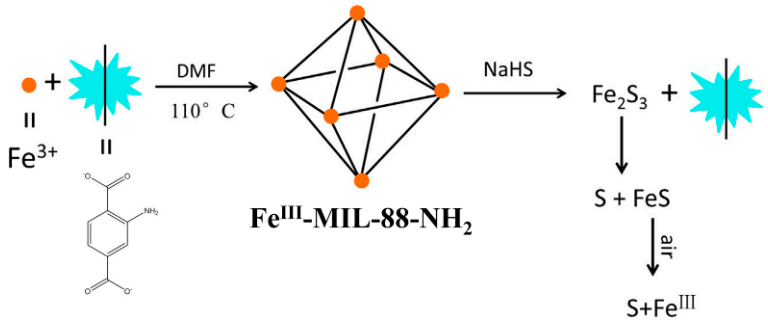

Figure 8. The synthesis and the turn-on fluoresence response of Fe^{III}-MIL-88-NH_2 for H_2S. Reproduced with permission from [87]. Copyright Elsevier B.V., New York, NY, USA, 2017.

2.2. MOF-Based Chemodosimeters for Biothiols

Biothiols such as Cys (cysteine), Hcy (homocysteine), and GSH (glutathione) play vital roles in various physiological and pathological processes [88–91]. During the past decade, a huge number of fluorescent probes have been developed for sensing and imaging biothiols by exploiting the specific reactivities of sulfhydryl group and/or amino group [92–98], including nucleophilic addition to electron-deficient unsaturated bonds, conjugate addition−cyclization reaction, cleavage of sulfonamide and sulfonate ester, cleavage of disulfide, and displacement of coordination to the metal complex. MOF-based Chemodosimeters for fluorescent sensing biothiols have emerged in the last two years.

Ghosh et al. reported a turn-on fluorescent probe, UiO-66-DNS, for selective sensing of biothiols [99]. UiO-66-DNS was prepared by post-grafting 2,4-dinitrosulfonyl moiety (DNS) to the chemically stable UiO-66-NH_2 MOF. UiO-66-DNS exhibited weak fluorescence due to the PET (photoinduced electron transfer) from the ligand of 2-aminoterephthalic acid to the highly electron-withdrawing functional group of DNP (Figure 9a). After the addition of Cys to a UiO-66-DNS dispersed water solution (Figure 9b), a significant enhancement (ca. ~48-fold) in luminescent intensity at 432 nm was obtained, which can be ascribed to the thiol-mediated cleavage of the DNS moiety and the release of UiO-66-NH_2. Compared with Cys, UiO-66-DNS displayed slower response toward GSH because of its intrinsic bulkier feature for diffusing and interacting with the probe. Other amino acids did not generate any obvious enhancement in the emission intensity of the probe (Figure 9c), which demonstrated that the UiO-66-DNS is highly specific to biothiol.

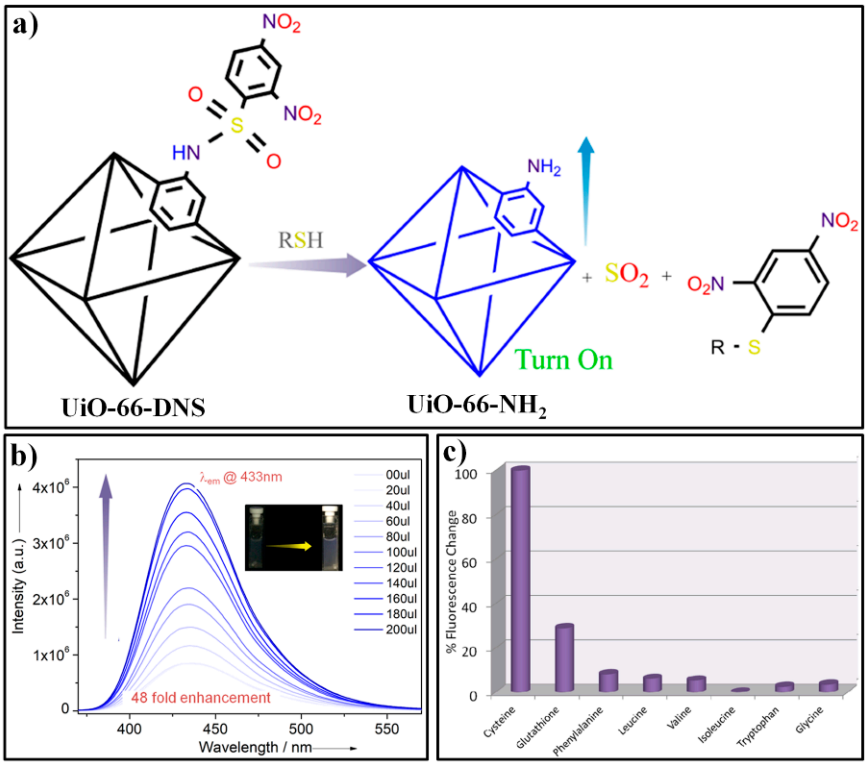

Figure 9. (**a**) The fluorescence detection mechanism of UiO-66-DNS for biothiols. (**b**) The fluorescence responses of UiO-66-DNS after addition of different amount of Cys. (**c**) Relative changes in the fluorescence intensity of UiO-66-DNS upon treatment with various amino acids. Reproduced with permission from [99]. Copyright American Chemical Society, 2016.

Wu et al. developed a novel aldehyde-functionalized MOF, Cd–PPCA (Figure 10a), for selective sensing of Hcy [100]. The Cd–PPCA consisted of a Cd(II) metal center and two types of ligands, H_3tca (4,4′,4″-tricarboxyltriphenylamine) and ppca (1H-pyrrolo-[2,3-*b*] pyridine-2-carbaldehyde). XRD (X-ray diffraction) results indicated that Cd–PPCA crystallized in the orthorhombic space group Pbnm with a = 25.500(5), b = 20.600(4), c = 13.700(3) Å (Figure 10b). Each unit building of trinuclear $[Cd_3(COO)_8]$ contained one ppca ligand, with a nitrogen atom to coordinate with Cd and a desired aldehyde functional group for the specific recognition of the target Hcy. Suspended in a HEPES (pH = 7.4) buffer solution, Cd–PPCA showed a weakened fluorescence emission at about 450 nm compared with similar MOFs comprised of H_3tca ligands and Cd^{2+} nods, which can be attributed to the PET from the triphenylamine groups to the electron withdrawing aldehyde moieties of the ppca ligand. With the addition of Hcy, the emission intensity of the assay showed a significant enhancement (Figure 10c), which can be ascribed to the selective reaction of the aldehyde moiety with Hcy and thus the inhibition of the PET process. This fluorescent response was also observed to be very fast (60 s) and sensitive (LOD: 40 nM). Moreover, the probe Cd–PPCA exhibited excellent specificity for Hcy over other species, including Cys (Figure 10d).

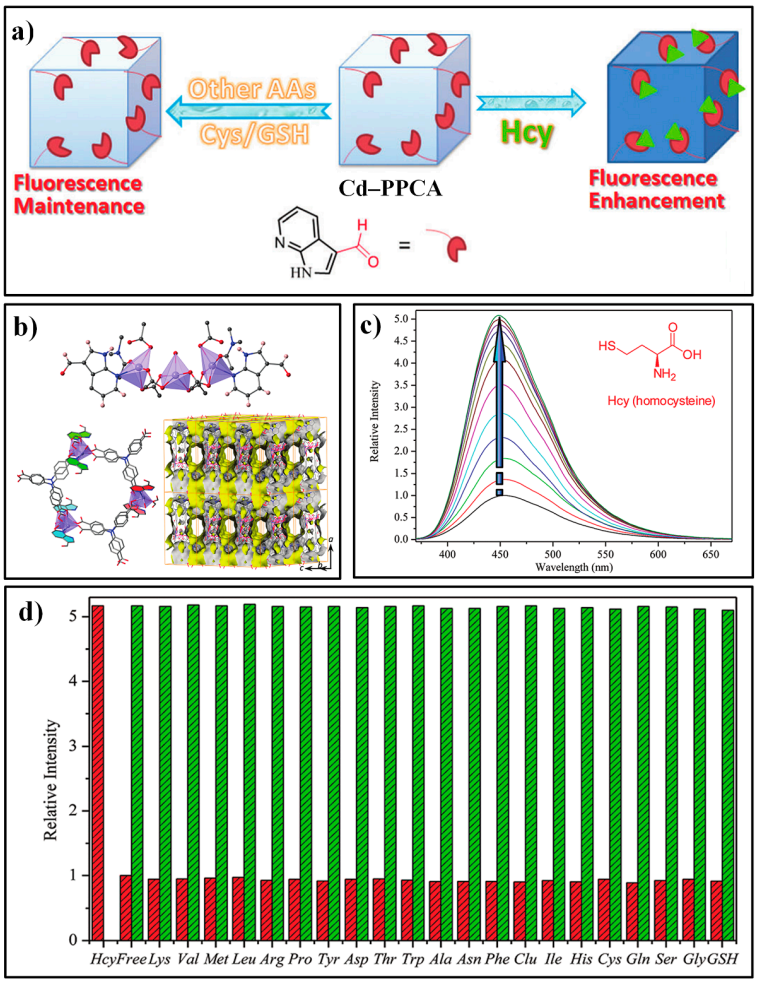

Figure 10. (**a**) The fluorescence detection mechanism of Cd–PPCA for Hcy. (**b**) the coordinated environment of the Cd^{2+} in Cd–PPCA (Top); a two-dimensional double-layer structure composed of Cd^{2+} and ligands of ppca and H_3tca (bottom-left); the Connolly surface of the framework of Cd–PPCA (bottom-right). (**c**) The fluorescence spectra of Cd–PPCA upon addition of different amounts of Hcy. (**d**) Results for selectivity and competition tests. Reproduced with permission from [100]. Copyright the Royal Society of Chemistry, 2018.

Wang and Zhang et al. developed a novel Zr-MOF based fluorescent PET switch/sensor, UiO-68-An/Ma [101]. The probe contains two kinds of ligands, one embedded with the anthracene unit serving as the luminophore and the other appended with a maleimide moiety as the PET acceptor (Figure 11a). The multivariate UiO-68-An/Ma favors a pseudo-PET process and only shows very weak fluorescence with an absolute PLQY (photoluminescence quantum yield) of 1.1%. Notably, the fluorescence behavior of UiO-68-An/Ma can be tuned by altering the acceptor moiety and thus the PET process. The authors firstly confirmed the tunable fluorescence response of UiO-68-An/Ma via a reversible D–A reaction with 3-furanmethanol. Furthermore, UiO-68-An/Ma was applied for sensing biothiols based on the well-established maleimide–thiol addition reaction. As a solid-state fluorescent turn-on sensor, UiO-68-An/Ma can sensitively response to biothiols (Cys, Hcy, and GSH) as low as 50 μM (Figure 11b).

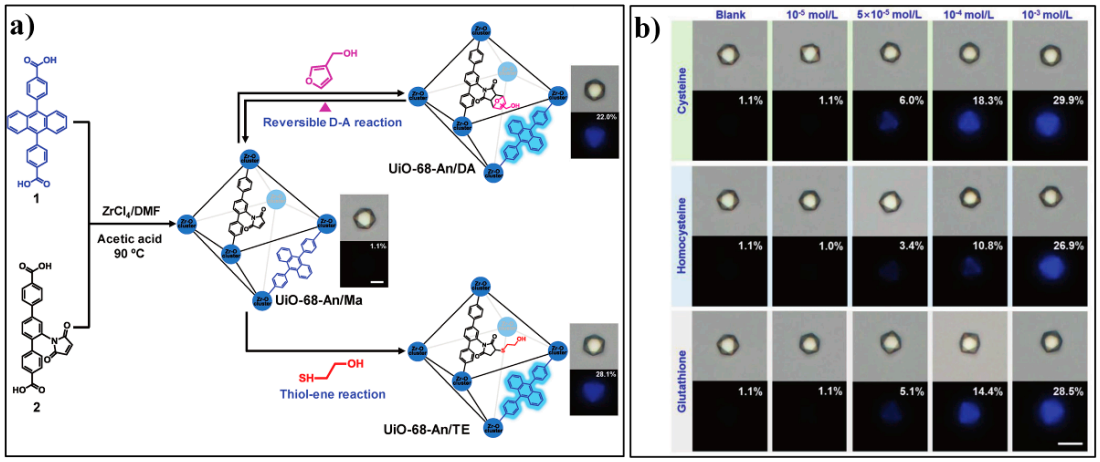

Figure 11. (**a**) Synthesis of UiO-68-An/Ma and tuning the fluorescent photoinduced electron transfer (PET) in the MOF through a reversible D–A reaction or thiol-ene reaction. (**b**) Bright-field and photoluminescence single-crystal images of UiO-68-An/Ma treated with different concentrations of Cys, Hcy, and GSH for 5 min. Reproduced with permission from [101]. Copyright Wiley-VCH, 2016.

With the in-situ encapsulation of rhodamine B (RhB) into Cu-BTC, Gao and Huang et al. reported a turn-on fluorescent assay (RhB@Cu-BTC MOFs) for sensing Cys [102]. The fluorescence of RhB@Cu-BTC was very weak because the embedded RhB was adjacent to the paramagnetic copper center. In the presence of Cys, the Cu-BTC framework collapsed, which resulted the release of RhB and thus a turn-on fluorescence response (Figure 12).

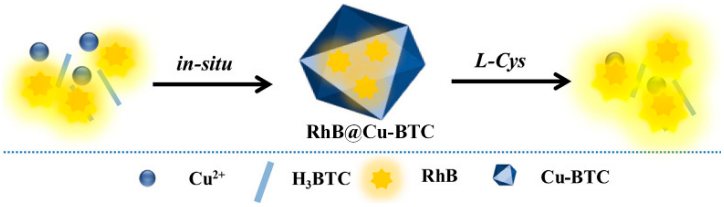

Figure 12. The synthesis of RhB@Cu-BTC and its sensing process for Cys. Reproduced with permission from [102]. Copyright 2018 Elsevier B.V., New York, NY, USA.

The MOF based fluorescent probe has also been exploited for sensing sulfur dioxide (SO_2) or sulfite/bisulfite, another kind of important sulfur-containing specie on both biological and environmental aspects. Ghosh et al. constructed a MOF based luminescent probe, NH_2-MIL-68(In)@CHO, for the monitoring of bisulfite [103]. The probe was prepared by the post synthetic approach via condensation of NH_2-MIL-68(In) (In(OH)(bdc-NH_2)) with glyoxal (Figure 13). The introduced aldehyde moiety can react with bisulfite to generate an OH group, which is available to form an intramolecular hydrogen bond and thus resulted in the inhibition of the C = N isomerization and the recovery of the fuorescence of the probe. Cui and Qian et al. prepared a Eu-BDC-NH_2 film on the UiO-66-NH_2 modified glass through an in situ secondary growth and successfully applied this functional film for sensing gaseous sulfur dioxide [104].

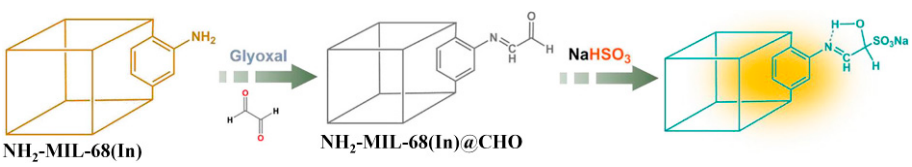

Figure 13. The synthesis of NH_2-MIL-68(In)@CHO and its sensing process for bisulfite. Reproduced with permission from [103]. Copyright Elsevier B.V., New York, NY, USA, 2018.

3. MOF-Based Chemodosimeters for Other Redox-Active Biomolecules

3.1. MOF-Based Chemodosimeters for HClO

Hypochlorous acid (HClO) is an important chemical reagent with wide application in various areas of organic synthesis, the cosmetics industry, food service, water treatment, etc. In living organisms, HClO is a kind of essential reactive oxygen species (ROS), which is normally produced in phagosomes via the reaction between hydrogen peroxide and chloride ions catalyzed by myeloperoxidase [105]. As a powerful oxidizer, the endogenous HClO can act as effective microbicidal agent when the host is being invaded by microbials [106]. On ther hand, HClO can also react with functioning biomolecules, such as proteins, nucleic acid, and fatty acids, which would produce adverse effects for organisms and correlate to numerous human diseases, such as kidney disease, cardiovascular diseases, and even cancers [107]. Therefore, the development of reliable analytical methods for monitoring HClO has attracted a great deal of attention [108,109]. Based on the unique characteristics of HClO, acting as both a potent oxidant and a good chlorination agent, various reaction-based organic fluorescent probes has been reported for selective sensing of HClO [110–117]. Until now, several examples of MOF-based chemodosimeters for luminescent detection of HClO have been presented.

Ma and Wang et al. developed the first MOF-based chemodosimetric probe for sensing HClO [118]. The designing strategy for the probe, UiO-Eu-L1 (L1: dimethyl 4-(carbaldehyde oxime) pyridine-2,6-dicarboxylate), is depicted in Figure 14. Uio-Eu-L1 was obtained by successively treating the Zr-MOF UiO-67 ($Zr_6O_4(OH)_4(BPDC)_6$) with europium ions and the functional ligand L1. Due to the efficient C = N isomerization-induced fluorescence quenching, UiO-Eu-L1 displayed very weak red emissions derived from europium ions. In the presence of HClO, the hydroxylamine moiety can be converted to aldehyde, which, in turn, leads to the inhibition of the C = N isomerization and thus the turn-on fluorescence response of the probe system. Ascribed to the long-lived phosphorescence of the Uio-Eu based MOF, this luminescent assay can efficiently eliminate the background signals and auto-fluorescence effects by the use of time-gated measurements. Uio-Eu-L1 also exhibited high sensitivity for HClO with a dynamic range of 0.1–5 μM and a detection limit of 16 nM.

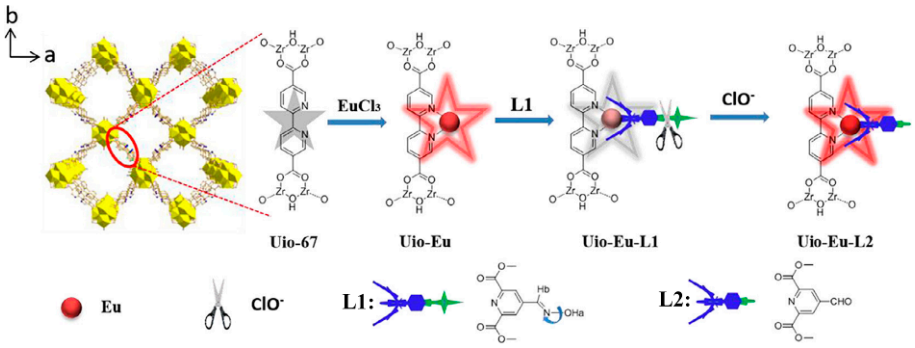

Figure 14. The structure and sensing mechanism of Uio-Eu-L1 for ClO^-. Reproduced with permission from [118]. Copyright Elsevier B.V., New York, NY, USA, 2018.

Gu et al. presented a novel luminophore integrated MOF system, AF@MOF-801, for specific detection of HClO [119]. The composite AF@MOF-801 can be readily prepared via a one-step process by using 5-aminofluorescein (AF) as a co-reactant in the synthesis of MOF-801 (Figure 15a). AF can serve as a sensitive turn-off fluorescent HClO probe, as HClO can react with AF to produce chlorinated products. However, other coexistent biological molecules (such as dopamine, DA) also can lead to the similar fluorescent changes of AF. In the constructed sensory platform of AF@MOF-801, AF can be confined in the cages of the framework and the target HClO can diffuse into the framework to react with the probe AF, while the ultra-small aperture can block the entry of large-sized interferents. Due to this size-selective effect, AF@MOF-801 displayed excellent specificity for HClO. Only ClO^- produced the significant luminescence response of AF@MOF-801 (Figure 15b), while both ClO^- and DA generated

strong fluorescence quenching for the free AF probe (Figure 15c). The feasibility of AF@MOF-801 for monitoring intracellular HClO was also demonstrated by MTT assay and flow cytometry analysis (FCA), as well as confocal laser scanning microscopy (CLSM) measurements (Figure 15d).

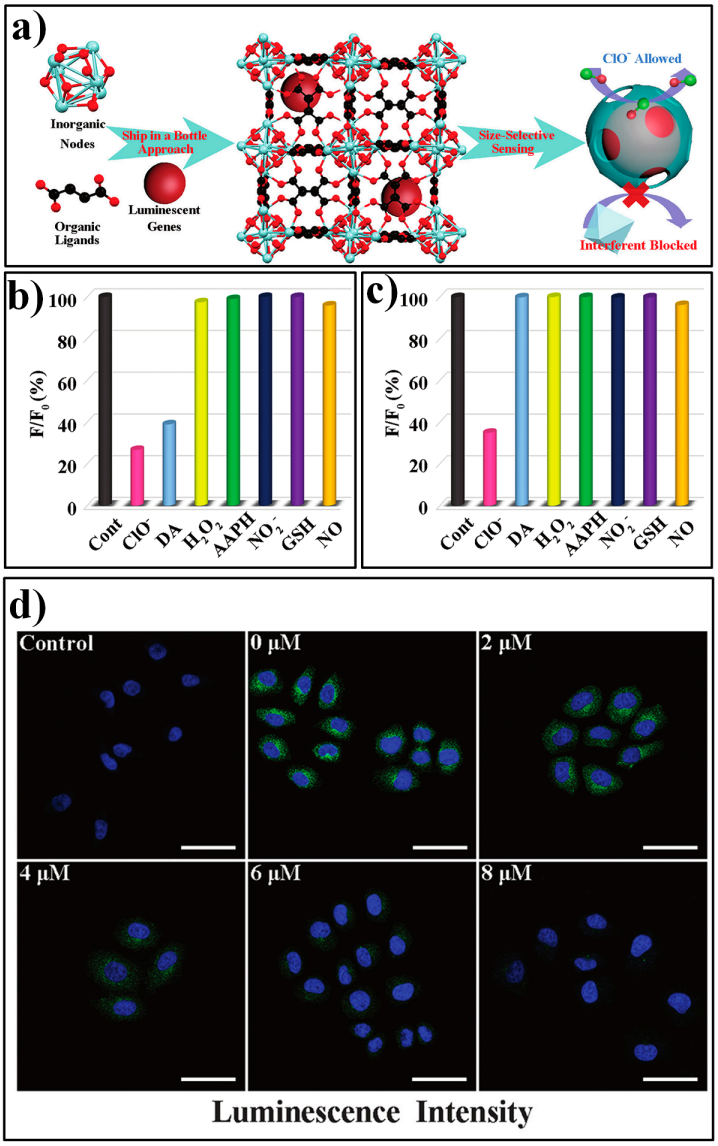

Figure 15. (**a**) Schematic illustration of the synthetic procedure for AF@MOF-801 and the size-selective sensing mechanism toward targe analyte of ClO^-. (**b**) The luminescence responses of free AF for various analytes. (**c**) The luminescence responses of AF@MOF-801 for various analytes. (**d**) The confocal laser scanning microscopy images of SMMC-7721 cells incubated with AF@MOF-801 and with various concentrations of ClO^-. Reproduced with permission from [119]. Copyright the Royal Society of Chemistry, 2019.

Chen et al. constructed a fluorophores@MOF (F1-Rubpy@ZnMOF74) nanocomposite-based ratiometric fluorescent probe for HClO by simultaneously encapsulating two fluorophores, fluorescein o-acrylate (F1) and tris(2,2′-bipyridyl)-dichroruthe-nium(II) hexahydrate (Rubpy), into ZnMOF74 [120]. F1-Rubpy@ZnMOF74 displayed two distinct emissions at 512 nm and 600 nm, corresponding to F1 and Rubpy, respectively. In the presence of HClO, the fluorescence of the target-responsive fluorophore F1 can be quenched, while the reference signal that originated from Rubpy remained unchanged, thus achieving a ratiometric response for HClO. In an aqueous HEPES buffer (pH = 7.5) solution, the

fluorescence intensity ratio (I_{512}/I_{600}) of the F1-Rubpy@ZnMOF74 was found to be linearly correlated with the concentration of ClO^- with a dynamic range of 3.6 nM-100 μM.

3.2. MOF-Based Chemodosimeters for Ascorbic Acid

Chen and Qian et. al. developed a Ce-MOF sensor ZJU-136-Ce, $(Me_2NH_2)_{0.6}\{[Ce^{IV}(TPTC)]_{0.4}$-$[Ce^{III}(TPTC)]_{0.6}\}(H_2O)_2$($H_4$TPTC = 1,1′:4′,1″-terphenyl-2′,4,4″,5′-tetracarboxylic acid) for sensing ascorbic acid (AA) [121]. Ce^{IV} in the probe ZJU-136-Ce can react with the AA to generate Ce^{III} and oxidized AA (DHA, dehydroascorbic acid). ZJU-136-Ce displays a luminescence band at 380 nm with a lifetime of 0.84 ns, which corresponds to the emissions of the Ce ion (Figure 16a). After reacting with AA, the probe system shows an increased emission band at about 400 nm (Figure 16b), which corresponds to the emission of the ligand. This fluorescence spectral response can be ascribed to the enhanced conjugation effect of the oxidized product DHA and thus the inhabited PET process from the TPTC ligand to the Ce ion. Subsequently, by introducing the Eu ions into the MOFs ZJU-136-Ce, the Qian group constructed a dual-emissive MOFs, ZJU-136-$Ce_{1-x}Eu_x$ (x = 0.24, 0.36), which can serve as an efficient ratiometric probe for monitoring AA [122]. The same research group also reported a new Zn-MOF, ZnL(H_2O) (ZJU-137, H_2L = 4,4′-(1H-pyrazole-1,3-diyl)dibenzoic acid, for the fluorescence "turn-off" detection of AA [123].

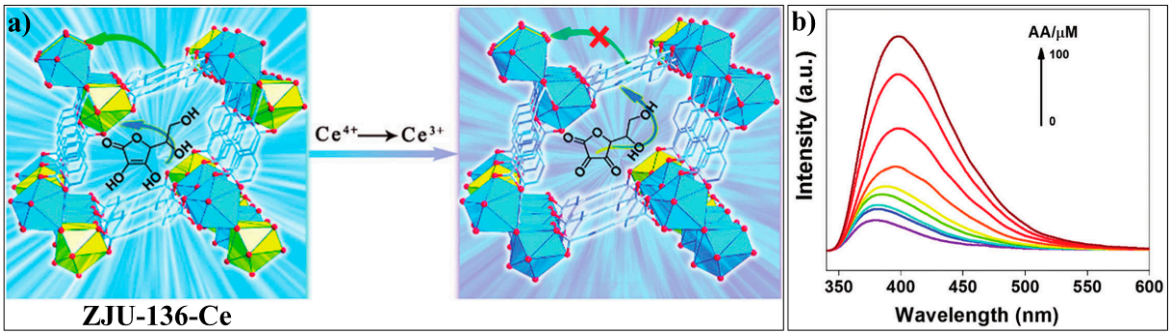

Figure 16. (**a**) Schematic illustration of the sensing mechanism of ZJU-136-Ce for asorbic acid (AA). (**b**) Luminescence spectra of ZJU-136-Ce in the presence of different concentrations of AA. Reproduced with permission from [121]. Copyright the Royal Society of Chemistry, 2017.

3.3. MOF-Based Chemodosimeter for 5-Hydroxytryptamine

Shi and Cheng et al. presented a Ln-MOF, Ln-MOF 1: $\{[Eu(TDA)(H_2BTEC)_{0.5}(H_2O)_3]\cdot H_2O\}_n$ (H_2TDA = thiazolidine 2,4-dicaboxylic acid, H_4btec = 1,2,4,5-benzenetetracarboxylic acid), for sensing 5-hydroxytryptamine (HT) and 5-hydroxyindole-3-acetic acid (HIAA), which was synthesized by reacting Eu^{3+} with mixed ligands of H_2TDA and H_4BTEC [124]. Ln-MOF 1 is crystallized in the monoclinic space group $P2_1/c$, in which each Eu^{3+} ion is nine-coordinates in a spherical capped square antiprism coordination geometry (Figure 17a). Due to the conjugated π system and the pronounced antenna effect of the ligand BTEC, Ln-MOF 1 displays intense characteristic emissions of the Eu^{3+} emitter with a maximum peak located at 616 nm, which is ascribed to the $^5D_0 \rightarrow {}^7F_2$ transition of Eu^{3+} ion. In the presence of HT or HIAA, the luminescence of the Ln-MOF 1 can be effectively quenched (Figure 17b,c). This process was attributed to the competitive absorption of excitation light by the analyte and the ligand. Ln-MOF 1 displayed several favorable features for HT and HIAA sensing, including high stability over a wide pH range and long-term storage, excellent sensitivity, and fast response time.

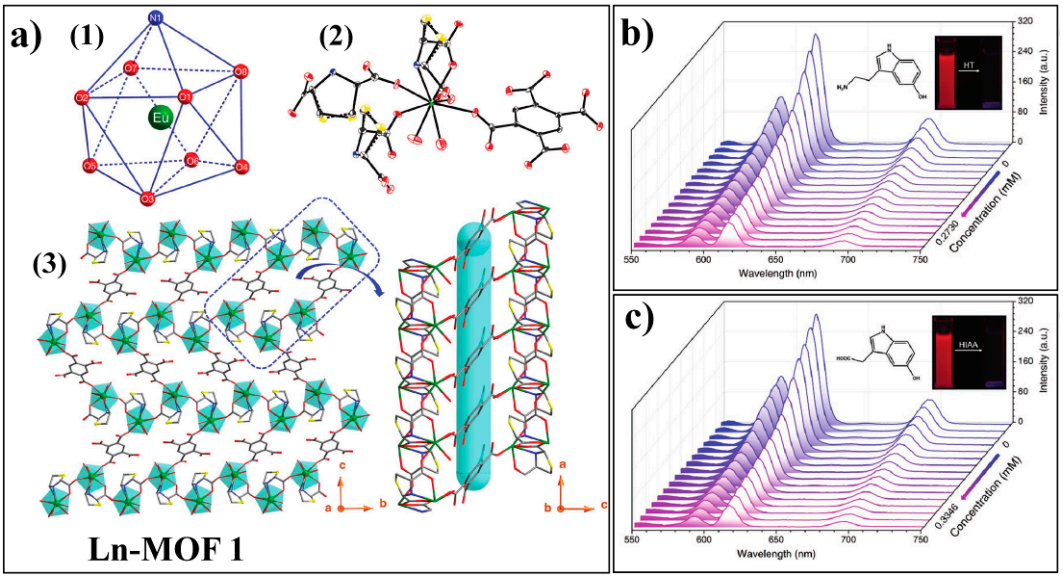

Figure 17. (**a**) structure of Ln-MOF 1: (1) Coordination geometry of the Eu^{3+}; (2) The asymmetric unit of Ln-MOF 1; (3) 3D framework composed of Ln-MOF 1. Atom codes: Eu (green), C (gray), N (blue), O (red), and S (yellow). Emission spectra of Ln-MOF 1 upon addition increase amount of (**b**) HT and (**c**) HIAA. Reproduced with permission from [124]. Copyright Wiley-VCH, 2018.

3.4. MOF-Based Chemodosimeter for H_2O_2

The hydrogen peroxide (H_2O_2) mediated conversion of arylboronates to phenols has been widely exploited for the development of fluorescent H_2O_2 probes [125]. On the basis of this unique chemical reaction, Biswas et al. developed a Zr-MOF based probe, Zr-UiO-66-B(OH)$_2$, for sensing H_2O_2 [126]. Zr-UiO-66-B(OH)$_2$, which can be can be easily prepared by reacting $ZrOCl_2 \cdot 8H_2O$ with the linker of BDC-B(OH)$_2$ (2-boronobenzene-1,4-dicarboxylic acid) (Figure 18). Zr-UiO-66-B(OH)$_2$ can act as a sensitive and selective off–on luminescent chemodosimeter for H_2O_2 with a 4-fold increment in the fluorescence intensity upon the addition of an excess amount of the target. Moreover, the probe Zr-UiO-66-B(OH)$_2$ was successfully applied to image H_2O_2 in MDAMB-231 cells.

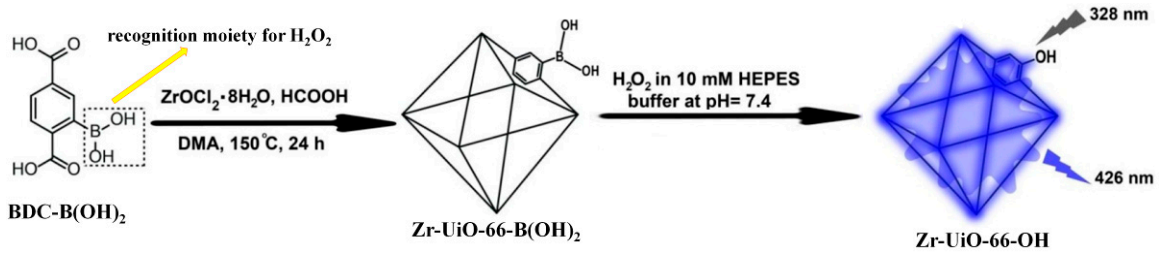

Figure 18. Schematic illustration of the sysnthesis of Zr-UiO-66-B(OH)$_2$ and the sensing process for H_2O_2. Reproduced with permission from [126]. Copyright American Chemical Society, 2018.

4. MOF-Based Chemodosimeters for Ions

4.1. MOF-Based Chemodosimeters for Fluoride Ions

The fluoride ion, F^-, as a typical hard Lewis base with the smallest ionic radius and highest charge density, has attracted much interest due to its association with various biological, medical, and technological processes. Commonly, fluoride is considered to be a critical component for preventing dental caries as fluoride can promote the formation of enamel-strengthening fluorapatite [127–129]. However, the over intake of fluoride can lead to excess mineralization within oganisms and cause gastric and kidney problems. Various analytical techniques have been developed for sensing fluoride [130],

including the well-established electrochemical method [131,132], chromatography [133,134], and colorimetric and fluorogenic assays [135]. In the past decades, numerous fluorescent probes have been developed for fluoride based on different fluoride-participated processes, such as fluoride-induced Si−O or Si−C bond cleavage, H−F hydrogen bonding formation, and Lewis acid−base interactions [136–138]. By exploiting these special reactivities of fluoride, several MOF-based luminesscent probes have recently been developed for its detection [139,140].

Yin et al. reported a reaction-based MOF probe (Eu-bop, $Eu_2(isp)_3(H_2O)_2$) for fluoride ions [141]. Eu-bop was prepared by using Eu^{3+} as the metal node and 5-bop (5-boronoisophthalic acid) as the ligand that contains a recognition moiety of a boric acid group for the target F^-. The substituted boric acid group also can tune the electronic structure of the ligand and resulted in an incomplete energy transfer from the ligand to Eu^{3+} emitter in the probe Eu-bop. Therefore, the Eu-bop displayed two emission bands: 366 nm, corresponding to the ligand of 5-bop; and 570–750 nm, corresponding to Eu^{3+}. Upon the addition of fluoride ions, the emission intensity at 366 nm was significant increased with a concomitant decrease in emissions at 625 nm (Figure 19a). The fluorescence response can be ascribed to the OH/F exchange reaction on the boron atom, which changed the hybridization state of boron from sp^2 ($-B(OH)_2$) to sp^3 ($-BF_3$), and thus disrupted the $p_\pi-\pi$ conjugation of the 5-bop and the decreased intersystem crossing efficiency (Figure 19b), as well as the antenna effect of the ligand. The fluorescence intensity ratio (I_{625}/I_{366}) of the probe system was found to vary linearly with the concentration of fluoride in a range of 4–80 μM. The probe was also applied to detect fluoride in real samples of river and underground water.

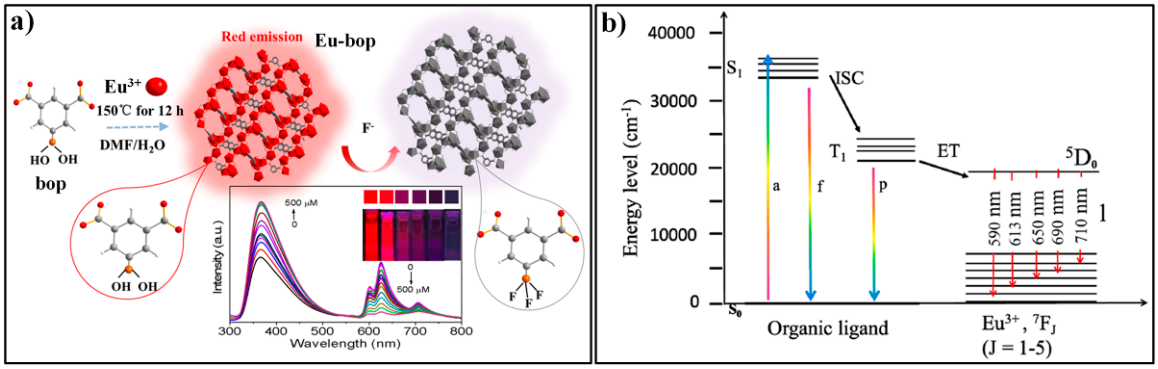

Figure 19. (**a**) The synthesis of Eu-bop and its sensing process for F^-. (**b**) Schematic representation of absorption, migration, and emission of Eu-bop. Reproduced with permission from [141]. Copyright American Chemical Society, 2017.

Recently, Stylianou et al. developed a luminescent lanthanide MOF, ([Eu(tctb)(H_2O)]·2DMF), referred to as SION-105 for the recognition of fluoride ion [142]. SION-105 consisted of tris (p-carboxylic acid) tridurylborane ligand ($tctb^{3-}$) and an Eu^{III} metal center. The ligand $tctb^{3-}$ contains a three-coordinate B acting as the recognition site for F^- and the surrounding duryl groups offering size-selective steric protection from other interferences (Figure 20a). SION-105 displayed a strong characteristic Eu^{III} luminescent emission due to the efficient antenna effect of the ligand $tctb^{3-}$ (Figure 20d). Upon the addition of F^-, the emissions of the probe can be quenched due to the specific interaction of F^- with the B Lewis acid site. A linear luminescence quenching response of SION-105 towards the F^- ion was observed in a range of 0.5 to 2.0 ppm (Figure 20b). A Stern−Volmer plot of quenching with the F^- concentration indicates the occurrence of both static and dynamic quenching (Figure 20c).

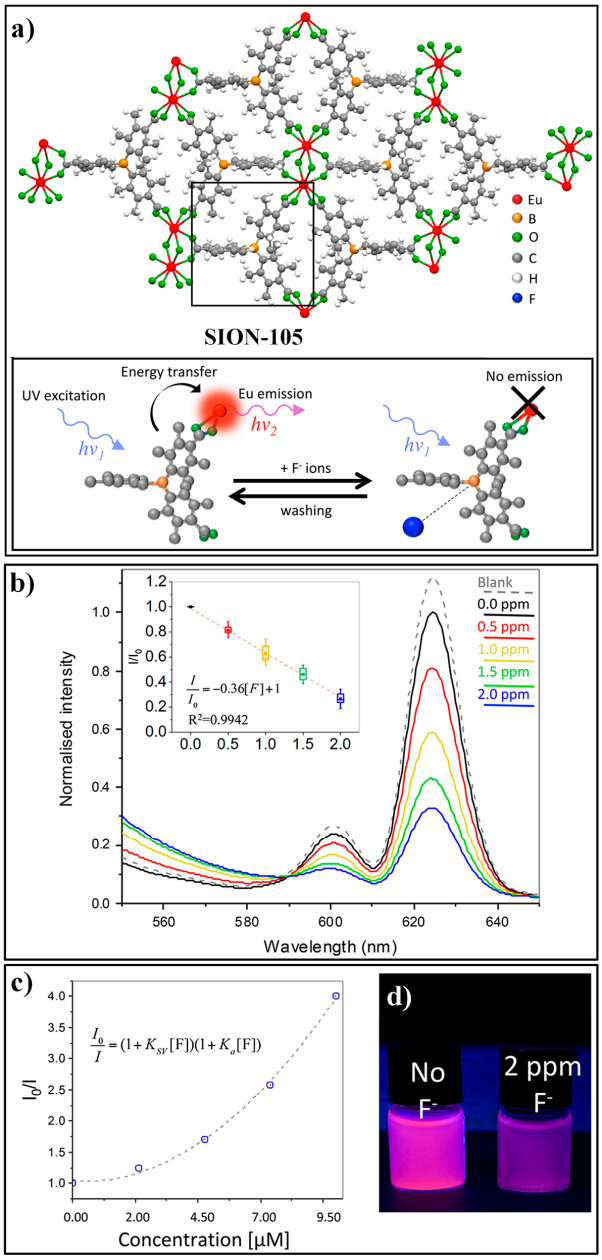

Figure 20. (**a**) The structure of SION-105 and its sensing process for F^-. (**b**) Luminescence spectra of SION-105 upon the addition of F^- with different concentrations. (**c**) Stern–Volmer plot of quenching with increasing F^- concentration. (**d**) Photographs of SION-105 suspension with or without of F^-. Reproduced with permission from [142]. Copyright American Chemical Society, 2019.

4.2. MOF-Based Chemodosimeter for Hg^{2+}

Mercury is one of the most toxic heavy metals in the environment. In aqueous media, mercury can be transformed into methylmercury, a powerful neurotoxin, which can be accumulated and ingested by humans through the food chain [143–145]. In the human body, methylmercury can lead to serious symptoms, such as cognitive and motor disorders, neurological impairments, brain damage, and even death [146–148]. These environmental and biological problems have prompted the rapid development of techniques for sensing mercury [149–153]. Until present, many reaction-based fluorescent probes for Hg^{2+} have been developed based on various Hg^{2+}-induced chemical processes [154–156], such as desulfation or deselenization processes, desulfation and cyclization processes, thiol elimination process, and the oxymercuration–elimination of vinyl/alkyne ether. Recently, Ghosh reported a MOF probe

(UiO-66@Butyne) for the reaction-based detection of Hg^{2+} [157]. UiO-66@Butyne was prepared from Zr ion and a ligand of 2,5-bis (but-3-yn-1-yloxy) terephthalic acid, which contained a butyne moiety acting as the recognition site for Hg^{2+} (Figure 21a). The prepared UiO-66@Butyne retained the crystalline structure of MOF UiO-66 and showed a strong green emission ($\lambda_{em,max}$ = 537 nm). Addition of Hg^{2+} to the aqueous solution of UiO-66@Butyne can result in fluorescent quenching of the system (Figure 21b), which can be attributed to the target-induced conversion of UiO-66@Butyne to the less fluorescent product of UiO-66@OH through the process of oxymercuration−elimination of ethynyl ether. As this MOF-based chemodosimeter exploited the specific reactivity of the target, UiO-66@OH exhibited excellent selectivity for Hg^{2+}.

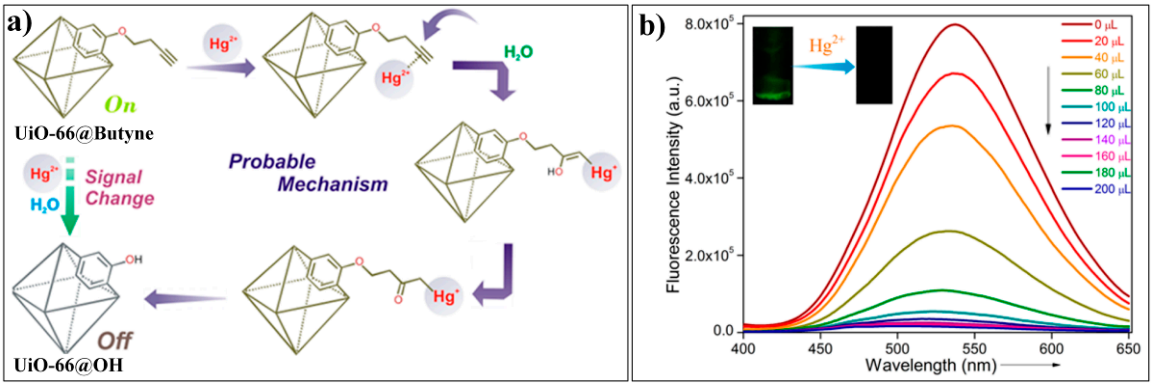

Figure 21. (**a**) Schematic illustration of the sensing mechanism of UiO-66@Butyne for Hg^{2+}. (**b**) Fluorescence spectra of UiO-66@Butyne upon addition of different amount of Hg^{2+}. Reproduced with permission from [157]. Copyright American Chemical Society, 2018.

4.3. MOF-Based Chemodosimeter for CN^-

The cyanide ion is an extremely poisonous chemical with widespread applications in industries such as metal mining, electroplating, and plastic and fertilizer manufacturing [158,159]. Various methods have been developed for the quantitative analysis of CN^-, including the titration method, electrochemical assays [160], chromatography [161], as well as the colorimetric and fluorogenic method [162]. Among these methods, the design and use of fluorescent probes for sensing CN^- have received considerable attention [163–165]. The chemososimeters for CN^- monitoring are normally associated, with several typical chemical reactions, including the cyanohydrin forming process, additions to the dicyano-vinyl group, michael addition, and indolium or pyridinium addition reactions. Recently, based on the specific addtion reaction of CN^- dicyano-vinyl group, Ghosh developed a Zeolitic imidazolate framework, M-ZIF-90 ($[Zn(C_8H_6N_4O_2)]_n$), for fluorescence sensing CN^- [166]. M-ZIF-90 was prepared by incorporating the recognition moiety of dicyano-vinyl onto the aldehyde-appended ZIF-90 via post-synthetic modification (Figure 22). In the H_2O/DMSO (1:1) mixture, M-ZIF-90 displayed a turn-off fluorescence response towards CN^- based on the nucleophilic addition of CN^- to the dicyano-vinyl group, which would interrupt the π-conjugation of the probe and thus result in significant fluorescence change.

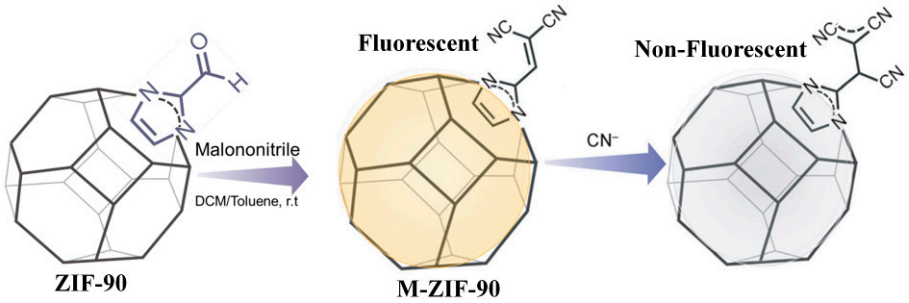

Figure 22. Schematic illustration of the the sysnthesis of M-ZIF-90 and the sensing process for CN^-. Reproduced with permission from [166]. Copyright Wiley-VCH, 2016.

5. Conclusions

In recent years, the design, synthesis, and application of MOFs have attracted an ever-increasing interest of researchers in the fields of chemistry, physics, materials, and engineering. The porous and crystalline nature, versatile selections for metal nodes and organic linkers, and tunable structures also endow MOFs with unique characteristics for sensing applications. In this review, we summarized recently developed MOF-based luminescent chemodosimeters. These reaction-based luminescent probes inherit the robust structural features of MOFs (e.g., large surface area, high porosity, and good thermal and chemical stability) and also exhibit excellent selectivity as they exploit the specific reactivities of the target analyte. Several strategies have been involved in the development of MOF-based chemodosimeters: (i) installing the recognition moiety onto the ligand via a post-synthetic modification approach or using a recognition moiety-appended ligand for preparing MOFs; (ii) construction of small-molecule fluorescent probe@MOF hybrid nanocomposites, in which the MOFs act as a carrier to confine the responsive probe; (iii) based on the target-induced collapse of the MOF structure, etc. Further, the MOF scaffolds exploited for constructing luminescent chemodosimeters are normally required to possess several features, including high stability and dispersibility in aqueous (or aqueous-containing) media, feasibility of installing the recognition moiety for certain analytes, environmental friendliness, and/or good biocompatibility for biosensing and bioimaging applications. Until now, although, dozens of MOF-based chemodosimeters have been reported for different analytes with several desirable traits, such as high selectivity and sensitivity, good stability, and rapid response, some critical performance limitations for this type of luminescent probe still need to be improved, including short-wavelength light excitation and/or emission, insufficient designing strategies for the probe, and limited target analytes. To overcome these shortcomings, several future directions for the design of MOF-based chemodosimeters are proposed herein.

(i) Employing New Rationally Designed Ligands

Most of the developed MOF-based chemodosimeters are ligand-based emission systems. Currently, the used ligand normally belongs to a blue-emissive fluorophore (e.g., BDC) with ultraviolet to blue light excitation, which is unfavorable for applications in complex samples, as well as in bioimaging. Future efforts should focus on the design and utilization of new ligands for constructing luminescent MOFs that have typical spectral features, such as visible/near-infrared emission, two-photon excitation, and large Stokes shifts.

(ii) Developing Dual-Ligand Mofs Systems

Compared with the single-ligand system, the dual-ligand MOFs have greater structural and functional diversity. For example, a fluorescence resonance energy transfer (FRET) sensing system could be achieved by carefully designing the electronic structure of two different ligands. Ratiometric fluorescent probes could be obtained by using one ligand as the target-responsive unit and the other ligand as the internal signal reference.

(iii) Expanding the Application Scope for Mof-Based Chemodosimeters

To date, MOF-based chemodosimeters have only been employed for sensing some ions and small molecules, such as F^-, Hg^{2+}, CN^-, H_2S, HClO, Cys, H_2O_2, AA, and HT. It is anticipated that future efforts will focus on developing MOF-based chemodosimeters for monitoring other important biomolecules, such as bioenzymes, as well as for bioimaging applications.

In summary, MOF-based luminescent chemodosimeters have increasingly attracted research interest. It can be expected that ongoing studies in this area will lead to the rapid development of more effective luminescent nanomaterials for sensing and imaging applications.

Author Contributions: Conceptualization, Y.H., Y.Z. (Yanli Zhou), and M.X.; Writing—Original Draft preparation, Y.H.; Writing—Review and Editing, S.C., Y.Z. (Yintang Zhang), Y.Z. (Yanli Zhou), and M.X.; project administration, Y.H., Y.Z. (Yanli Zhou), and M.X.; funding acquisition, Y.H., Y.Z. (Yanli Zhou), and M.X.

Funding: This work was funded by the National Natural Science Foundation of China (Project Nos. 21804085, 21675109, U1404215, 21475084).

Conflicts of Interest: The authors declare no conflict of interest.

Abbreviations

IPA	isophthalic acid
NDC	napthalene-2,6-dicarboxylic acid
TCPP	*meso*-tetrakis (4-carboxylphenyl) porphyrin
HBSS	Hanks' balanced salt solutions
BBS	boricacid−borax buffer
SNP	*S*-nitroso-*N*-acetyl-DL-penicillamine
PPG	DL-propargylglycine
TO	thiazole orange
MTT	3-(4,5-dimethylthiazol-2-yl)-2,5-diphenyltetrazolium bromide
FCA	flow cytometry analysis
CLSM	confocal laser scanning microscopy
Cys	cysteine
Hcy	homocysteine
GSH	glutathione
DNP	dinitrophenyl
PET	photoinduced electron transfer
H3tca	4,4′,4″-tricarboxyltriphenylamine
Ppca	1H-pyrrolo-[2,3-*b*]pyridine-2-carbaldehyde
PLQY	photoluminescence quantum yield
RhB	rhodamine B
AA	ascorbic acid
Isp	isophthalic acid
5-bop	5-boronoisophthalic acid
H_3tctb	tris (p-carboxylic acid) tridurylborane
H_2TDA	thiazolidine 2,4-dicaboxylic acid
BDC-B$(OH)_2$	2-boronobenzene-1,4-dicarboxylic acid
ZIF	Zeolitic imidazolate frameworks

References

1. Li, H.; Eddaoudi, M.; O'Keeffe, M.; Yaghi, O.M. Design and synthesis of an exceptionally stable and highly porous metal-organic framework. *Nature* **1999**, *402*, 276–279. [CrossRef]
2. James, S.L. Metal-organic frameworks. *Chem. Soc. Rev.* **2003**, *32*, 276–288. [CrossRef] [PubMed]
3. Stock, N.; Biswas, S. Synthesis of Metal-Organic Frameworks (MOFs): Routes to Various MOF Topologies, Morphologies, and Composites. *Chem. Rev.* **2012**, *112*, 933–969. [CrossRef] [PubMed]

4. Rowsell, J.L.C.; Yaghi, O.M. Metal-organic frameworks: A new class of porous materials. *Microporous Mesoporous Mater.* **2004**, *73*, 3–14. [CrossRef]
5. Cook, T.R.; Zheng, Y.R.; Stang, P.J. Metal-Organic Frameworks and Self-Assembled Supramolecular Coordination Complexes: Comparing and Contrasting the Design, Synthesis, and Functionality of Metal-Organic Materials. *Chem. Rev.* **2013**, *113*, 734–777. [CrossRef] [PubMed]
6. Li, J.R.; Kuppler, R.J.; Zhou, H.C. Selective gas adsorption and separation in metal-organic frameworks. *Chem. Soc. Rev.* **2009**, *38*, 1477–1504. [CrossRef]
7. Li, J.R.; Ma, Y.G.; McCarthy, M.C.; Sculley, J.; Yu, J.M.; Jeong, H.K.; Balbuena, P.B.; Zhou, H.C. Carbon dioxide capture-related gas adsorption and separation in metal-organic frameworks. *Coord. Chem. Rev.* **2011**, *255*, 1791–1823. [CrossRef]
8. Wang, Z.; Luo, X.; Zheng, B.; Huang, L.; Hang, C.; Jiao, Y.; Cao, X.; Zeng, W.; Yun, R. Highly Selective Carbon Dioxide Capture and Cooperative Catalysis of a Water-Stable Acylamide-Functionalized Metal–Organic Framework. *Eur. J. Inorg. Chem.* **2018**, *2018*, 1309–1314. [CrossRef]
9. Zheng, B.; Luo, X.; Wang, Z.; Zhang, S.; Yun, R.; Huang, L.; Zeng, W.; Liu, W. An unprecedented water stable acylamide-functionalized metal–organic framework for highly efficient CH_4/CO_2 gas storage/separation and acid–base cooperative catalytic activity. *Inorg. Chem. Front.* **2018**, *5*, 2355–2363. [CrossRef]
10. Zheng, B.; Huang, L.; Cao, X.; Shen, S.; Cao, H.; Hang, C.; Zeng, W.; Wang, Z. A highly porous acylamide decorated MOF-505 analogue exhibiting high and selective CO_2 gas uptake capability. *CrystEngComm* **2018**, *20*, 1874–1881. [CrossRef]
11. Zheng, B.; Wang, H.; Wang, Z.; Ozaki, N.; Hang, C.; Luo, X.; Huang, L.; Zeng, W.; Yang, M.; Duan, J. A highly porous rht-type acylamide-functionalized metal–organic framework exhibiting large CO_2 uptake capabilities. *Chem. Commun.* **2016**, *52*, 12988–12991. [CrossRef] [PubMed]
12. Lee, J.; Farha, O.K.; Roberts, J.; Scheidt, K.A.; Nguyen, S.T.; Hupp, J.T. Metal-organic framework materials as catalysts. *Chem. Soc. Rev.* **2009**, *38*, 1450–1459. [CrossRef] [PubMed]
13. Liu, J.W.; Chen, L.F.; Cui, H.; Zhang, J.Y.; Zhang, L.; Su, C.Y. Applications of metal-organic frameworks in heterogeneous supramolecular catalysis. *Chem. Soc. Rev.* **2014**, *43*, 6011–6061. [CrossRef] [PubMed]
14. Corma, A.; Garcia, H.; Xamena, F. Engineering Metal Organic Frameworks for Heterogeneous Catalysis. *Chem. Rev.* **2010**, *110*, 4606–4655. [CrossRef] [PubMed]
15. Li, H.; Ke, F.; Zhu, J. MOF-Derived Ultrathin Cobalt Phosphide Nanosheets as Efficient Bifunctional Hydrogen Evolution Reaction and Oxygen Evolution Reaction Electrocatalysts. *Nanomaterials* **2018**, *8*, 89. [CrossRef] [PubMed]
16. Horcajada, P.; Gref, R.; Baati, T.; Allan, P.K.; Maurin, G.; Couvreur, P.; Ferey, G.; Morris, R.E.; Serre, C. Metal-Organic Frameworks in Biomedicine. *Chem. Rev.* **2012**, *112*, 1232–1268. [CrossRef]
17. Illes, B.; Wuttke, S.; Engelke, H. Liposome-Coated Iron Fumarate Metal-Organic Framework Nanoparticles for Combination Therapy. *Nanomaterials* **2017**, *7*, 351. [CrossRef] [PubMed]
18. Kreno, L.E.; Leong, K.; Farha, O.K.; Allendorf, M.; Van Duyne, R.P.; Hupp, J.T. Metal-Organic Framework Materials as Chemical Sensors. *Chem. Rev.* **2012**, *112*, 1105–1125. [CrossRef]
19. Hu, Z.C.; Deibert, B.J.; Li, J. Luminescent metal-organic frameworks for chemical sensing and explosive detection. *Chem. Soc. Rev.* **2014**, *43*, 5815–5840. [CrossRef]
20. Allendorf, M.D.; Bauer, C.A.; Bhakta, R.K.; Houk, R.J.T. Luminescent metal-organic frameworks. *Chem. Soc. Rev.* **2009**, *38*, 1330–1352. [CrossRef]
21. Cui, Y.J.; Yue, Y.F.; Qian, G.D.; Chen, B.L. Luminescent Functional Metal-Organic Frameworks. *Chem. Rev.* **2012**, *112*, 1126–1162. [CrossRef] [PubMed]
22. Zhang, Y.M.; Yuan, S.; Day, G.; Wang, X.; Yang, X.Y.; Zhou, H.C. Luminescent sensors based on metal-organic frameworks. *Coord. Chem. Rev.* **2018**, *354*, 28–45. [CrossRef]
23. Wang, Y.; Lin, S.; Luo, J.; Huang, R.; Cai, H.; Yan, W.; Yang, H. A Novel Tb@Sr-MOF as Self-Calibrating Luminescent Sensor for Nutritional Antioxidant. *Nanomaterials* **2018**, *8*, 796. [CrossRef] [PubMed]
24. Lustig, W.P.; Mukherjee, S.; Rudd, N.D.; Desai, A.V.; Li, J.; Ghosh, S.K. Metal–organic frameworks: Functional luminescent and photonic materials for sensing applications. *Chem. Soc. Rev.* **2017**, *46*, 3242–3285. [CrossRef] [PubMed]
25. Wang, H.; Lustig, W.P.; Li, J. Sensing and capture of toxic and hazardous gases and vapors by metal-organic frameworks. *Chem. Soc. Rev.* **2018**, *47*, 4729–4756. [CrossRef] [PubMed]

26. Liu, X.G.; Wang, H.; Chen, B.; Zou, Y.; Gu, Z.G.; Zhao, Z.J.; Shen, L. A luminescent metal-organic framework constructed using a tetraphenylethene-based ligand for sensing volatile organic compounds. *Chem. Commun.* **2015**, *51*, 1677–1680. [CrossRef] [PubMed]
27. Zhang, M.; Feng, G.; Song, Z.; Zhou, Y.-P.; Chao, H.-Y.; Yuan, D.; Tan, T.T.Y.; Guo, Z.; Hu, Z.; Tang, B.Z.; et al. Two-Dimensional Metal–Organic Framework with Wide Channels and Responsive Turn-On Fluorescence for the Chemical Sensing of Volatile Organic Compounds. *J. Am. Chem. Soc.* **2014**, *136*, 7241–7244. [CrossRef]
28. Hao, J.N.; Yan, B. Highly sensitive and selective fluorescent probe for Ag^{+} based on a Eu^{3+} post-functionalized metal-organic framework in aqueous media. *J. Mater. Chem. A* **2014**, *2*, 18018–18025. [CrossRef]
29. Yang, C.X.; Ren, H.B.; Yan, X.P. Fluorescent Metal Organic Framework MIL-53(Al) for Highly Selective and Sensitive Detection of Fe3+ in Aqueous Solution. *Anal. Chem.* **2013**, *85*, 7441–7446. [CrossRef]
30. Zhang, Y.; Yan, B. A ratiometric fluorescent sensor with dual response of Fe^{3+}/Cu^{2+} based on europium post-modified sulfone-metal-organic frameworks and its logical application. *Talanta* **2019**, *197*, 291–298. [CrossRef]
31. Helal, A.; Nguyen, H.L.; Al-Ahmed, A.; Cordova, K.E.; Yamani, Z.H. An Ultrasensitive and Selective Metal–Organic Framework Chemosensor for Palladium Detection in Water. *Inorg. Chem.* **2019**, *58*, 1738–1741. [CrossRef] [PubMed]
32. Wu, P.Y.; Wang, J.; He, C.; Zhang, X.L.; Wang, Y.T.; Liu, T.; Duan, C.Y. Luminescent Metal-Organic Frameworks for Selectively Sensing Nitric Oxide in an Aqueous Solution and in Living Cells. *Adv. Funct. Mater.* **2012**, *22*, 1698–1703. [CrossRef]
33. Liu, S.-Y.; Qi, X.-L.; Lin, R.-B.; Cheng, X.-N.; Liao, P.-Q.; Zhang, J.-P.; Chen, X.-M. Porous Cu(I) Triazolate Framework and Derived Hybrid Membrane with Exceptionally High Sensing Efficiency for Gaseous Oxygen. *Adv. Funct. Mater.* **2014**, *24*, 5866–5872. [CrossRef]
34. Xu, Y.; Liu, S.-Y.; Liu, J.; Zhang, L.; Chen, D.; Chen, J.; Ma, Y.; Zhang, J.-P.; Dai, Z.; Zou, X. In Situ Enzyme Immobilization with Oxygen-Sensitive Luminescent Metal–Organic Frameworks to Realize "All-in-One" Multifunctions. *Chem. Eur. J.* **2019**, *25*, 5463–5471. [CrossRef] [PubMed]
35. Lin, R.-B.; Liu, S.-Y.; Ye, J.-W.; Li, X.-Y.; Zhang, J.-P. Photoluminescent Metal–Organic Frameworks for Gas Sensing. *Adv. Sci.* **2016**, *3*, 1500434. [CrossRef] [PubMed]
36. Lu, Y.; Yan, B. A ratiometric fluorescent pH sensor based on nanoscale metal–organic frameworks (MOFs) modified by europium(III) complexes. *Chem. Commun.* **2014**, *50*, 13323–13326. [CrossRef] [PubMed]
37. Harbuzaru, B.V.; Corma, A.; Rey, F.; Jordá, J.L.; Ananias, D.; Carlos, L.D.; Rocha, J. A Miniaturized Linear pH Sensor Based on a Highly Photoluminescent Self-Assembled Europium(III) Metal–Organic Framework. *Angew. Chem. Int. Ed.* **2009**, *48*, 6476–6479. [CrossRef]
38. Zhang, X.; Jiang, K.; He, H.; Yue, D.; Zhao, D.; Cui, Y.; Yang, Y.; Qian, G. A stable lanthanide-functionalized nanoscale metal-organic framework as a fluorescent probe for pH. *Sens. Actuators B Chem.* **2018**, *254*, 1069–1077. [CrossRef]
39. Chen, H.; Wang, J.; Shan, D.; Chen, J.; Zhang, S.; Lu, X. Dual-Emitting Fluorescent Metal–Organic Framework Nanocomposites as a Broad-Range pH Sensor for Fluorescence Imaging. *Anal. Chem.* **2018**, *90*, 7056–7063. [CrossRef]
40. He, C.B.; Lu, K.D.; Lin, W.B. Nanoscale Metal-Organic Frameworks for Real-Time Intracellular pH Sensing in Live Cells. *J. Am. Chem. Soc.* **2014**, *136*, 12253–12256. [CrossRef]
41. Jiang, H.L.; Feng, D.W.; Wang, K.C.; Gu, Z.Y.; Wei, Z.W.; Chen, Y.P.; Zhou, H.C. An Exceptionally Stable, Porphyrinic Zr Metal-Organic Framework Exhibiting pH-Dependent Fluorescence. *J. Am. Chem. Soc.* **2013**, *135*, 13934–13938. [CrossRef] [PubMed]
42. Holler, C.J.; Muller-Buschbaum, K. The First Dinitrile Frameworks of the Rare Earth Elements: (3)(infinity) LnCl(3)(1,4-Ph(CN)(2)) and (3)(infinity) Ln(2)Cl(6)(1,4-Ph(CN)(2)), Ln = Sm, Gd, Tb, Y; Access to Novel Metal-Organic Frameworks by Solvent Free Synthesis in Molten 1,4-Benzodinitrile. *Inorg. Chem.* **2008**, *47*, 10141–10149. [CrossRef] [PubMed]
43. Marshall, R.J.; Kalinovskyy, Y.; Griffin, S.L.; Wilson, C.; Blight, B.A.; Forgan, R.S. Functional Versatility of a Series of Zr Metal–Organic Frameworks Probed by Solid-State Photoluminescence Spectroscopy. *J. Am. Chem. Soc.* **2017**, *139*, 6253–6260. [CrossRef] [PubMed]
44. Robinson, A.L.; Stavila, V.; Zeitler, T.R.; White, M.I.; Thornberg, S.M.; Greathouse, J.A.; Allendorf, M.D. Ultrasensitive Humidity Detection Using Metal–Organic Framework-Coated Microsensors. *Anal. Chem.* **2012**, *84*, 7043–7051. [CrossRef] [PubMed]

45. Gao, Y.; Jing, P.T.; Yan, N.; Hilbers, M.; Zhang, H.; Rothenberg, G.; Tanase, S. Dual-mode humidity detection using a lanthanide-based metal-organic framework: Towards multifunctional humidity sensors. *Chem. Commun.* **2017**, *53*, 4465–4468. [CrossRef] [PubMed]
46. Zhao, D.; Yue, D.; Jiang, K.; Zhang, L.; Li, C.X.; Qian, G.D. Isostructural Tb^{3+}/Eu^{3+} Co-Doped Metal Organic Framework Based on Pyridine-Containing Dicarboxylate Ligands for Ratiometric Luminescence Temperature Sensing. *Inorg. Chem.* **2019**, *58*, 2637–2644. [CrossRef] [PubMed]
47. Li, H.; Han, W.; Lv, R.; Zhai, A.; Li, X.L.; Gu, W.; Liu, X. Dual-Function Mixed-Lanthanide Metal-Organic Framework for Ratiometric Water Detection in Bioethanol and Temperature Sensing. *Anal. Chem.* **2019**, *91*, 2148–2154. [CrossRef]
48. Wieme, J.; Lejaeghere, K.; Kresse, G.; Van Speybroeck, V. Tuning the balance between dispersion and entropy to design temperature-responsive flexible metal-organic frameworks. *Nat. Commun.* **2018**, *9*, 10. [CrossRef]
49. Kimura, H.; Nagai, Y.; Umemura, K.; Kimura, Y. Physiological Roles of Hydrogen Sulfide: Synaptic Modulation, Neuroprotection, and Smooth Muscle Relaxation. *Antioxid. Redox Signal.* **2005**, *7*, 795–803. [CrossRef]
50. Li, L.; Rose, P.; Moore, P.K. Hydrogen Sulfide and Cell Signaling. *Annu. Rev. Pharmacool. Toxicol.* **2011**, *51*, 169–187. [CrossRef]
51. Watanabe, M.; Osada, J.; Aratani, Y.; Kluckman, K.; Reddick, R.; Malinow, M.R.; Maeda, N. Mice deficient in cystathionine beta-synthase: Animal models for mild and severe homocyst(e)inemia. *Proc. Natl. Acad. Sci. USA* **1995**, *92*, 1585–1589. [CrossRef] [PubMed]
52. Dorman, D.C.; Moulin, F.J.-M.; McManus, B.E.; Mahle, K.C.; James, R.A.; Struve, M.F. Cytochrome Oxidase Inhibition Induced by Acute Hydrogen Sulfide Inhalation: Correlation with Tissue Sulfide Concentrations in the Rat Brain, Liver, Lung, and Nasal Epithelium. *Toxicol. Sci.* **2002**, *65*, 18–25. [CrossRef] [PubMed]
53. Xu, T.L.; Scafa, N.; Xu, L.P.; Zhou, S.F.; Al-Ghanem, K.A.; Mahboob, S.; Fugetsu, B.; Zhang, X.J. Electrochemical hydrogen sulfide biosensors. *Analyst* **2016**, *141*, 1185–1195. [CrossRef] [PubMed]
54. Llobet, E.; Brunet, J.; Pauly, A.; Ndiaye, A.; Varenne, C. Nanomaterials for the Selective Detection of Hydrogen Sulfide in Air. *Sensors* **2017**, *17*, 19. [CrossRef] [PubMed]
55. Luo, Y.N.; Zhu, C.Z.; Du, D.; Lin, Y.H. A review of optical probes based on nanomaterials for the detection of hydrogen sulfide in biosystems. *Anal. Chim. Acta* **2019**, *1061*, 1–12. [CrossRef] [PubMed]
56. Lin, V.S.; Chen, W.; Xian, M.; Chang, C.J. Chemical probes for molecular imaging and detection of hydrogen sulfide and reactive sulfur species in biological systems. *Chem. Soc. Rev.* **2015**, *44*, 4596–4618. [CrossRef] [PubMed]
57. Hao, Y.; Zhang, Y.; Ruan, K.; Meng, F.; Li, T.; Guan, J.; Du, L.; Qu, P.; Xu, M. A highly selective long-wavelength fluorescent probe for hydrazine and its application in living cell imaging. *Spectrochim. Acta A* **2017**, *184*, 355–360. [CrossRef]
58. Hao, Y.; Zhang, Y.; Ruan, K.; Chen, W.; Zhou, B.; Tan, X.; Wang, Y.; Zhao, L.; Zhang, G.; Qu, P.; et al. A naphthalimide-based chemodosimetric probe for ratiometric detection of hydrazine. *Sens. Actuators B Chem.* **2017**, *244*, 417–424. [CrossRef]
59. Yu, F.; Han, X.; Chen, L. Fluorescent probes for hydrogen sulfide detection and bioimaging. *Chem. Commun.* **2014**, *50*, 12234–12249. [CrossRef]
60. Peng, H.; Cheng, Y.; Dai, C.; King, A.L.; Predmore, B.L.; Lefer, D.J.; Wang, B. A Fluorescent Probe for Fast and Quantitative Detection of Hydrogen Sulfide in Blood. *Angew. Chem. Int. Ed.* **2011**, *50*, 9672–9675. [CrossRef]
61. Lippert, A.R.; New, E.J.; Chang, C.J. Reaction-Based Fluorescent Probes for Selective Imaging of Hydrogen Sulfide in Living Cells. *J. Am. Chem. Soc.* **2011**, *133*, 10078–10080. [CrossRef] [PubMed]
62. Hammers, M.D.; Taormina, M.J.; Cerda, M.M.; Montoya, L.A.; Seidenkranz, D.T.; Parthasarathy, R.; Pluth, M.D. A Bright Fluorescent Probe for H_2S Enables Analyte-Responsive, 3D Imaging in Live Zebrafish Using Light Sheet Fluorescence Microscopy. *J. Am. Chem. Soc.* **2015**, *137*, 10216–10223. [CrossRef] [PubMed]
63. Ke, B.; Wu, W.; Liu, W.; Liang, H.; Gong, D.; Hu, X.; Li, M. Bioluminescence Probe for Detecting Hydrogen Sulfide in Vivo. *Anal. Chem.* **2016**, *88*, 592–595. [CrossRef] [PubMed]
64. Chen, Y.; Zhu, C.; Yang, Z.; Chen, J.; He, Y.; Jiao, Y.; He, W.; Qiu, L.; Cen, J.; Guo, Z. A Ratiometric Fluorescent Probe for Rapid Detection of Hydrogen Sulfide in Mitochondria. *Angew. Chem. Int. Ed.* **2013**, *52*, 1688–1691. [CrossRef] [PubMed]

65. Wang, X.; Sun, J.; Zhang, W.; Ma, X.; Lv, J.; Tang, B. A near-infrared ratiometric fluorescent probe for rapid and highly sensitive imaging of endogenous hydrogen sulfide in living cells. *Chem. Sci.* **2013**, *4*, 2551–2556. [CrossRef]
66. Huang, Z.; Ding, S.; Yu, D.; Huang, F.; Feng, G. Aldehyde group assisted thiolysis of dinitrophenyl ether: A new promising approach for efficient hydrogen sulfide probes. *Chem. Commun.* **2014**, *50*, 9185–9187. [CrossRef] [PubMed]
67. Men, J.; Yang, X.; Zhang, H.; Zhou, J. A near-infrared fluorescent probe based on nucleophilic substitution–cyclization for selective detection of hydrogen sulfide and bioimaging. *Dyes Pigments* **2018**, *153*, 206–212. [CrossRef]
68. Sasakura, K.; Hanaoka, K.; Shibuya, N.; Mikami, Y.; Kimura, Y.; Komatsu, T.; Ueno, T.; Terai, T.; Kimura, H.; Nagano, T. Development of a Highly Selective Fluorescence Probe for Hydrogen Sulfide. *J. Am. Chem. Soc.* **2011**, *133*, 18003–18005. [CrossRef]
69. Liang, Z.H.; Tsoi, T.H.; Chan, C.F.; Dai, L.X.; Wu, Y.D.; Du, G.Y.; Zhu, L.Z.; Lee, C.S.; Wong, W.T.; Law, G.L.; et al. A smart "off-on" gate for the in situ detection of hydrogen sulphide with Cu(II)-assisted europium emission. *Chem. Sci.* **2016**, *7*, 2151–2156. [CrossRef] [PubMed]
70. Vikrant, K.; Kumar, V.; Ok, Y.S.; Kim, K.-H.; Deep, A. Metal-organic framework (MOF)-based advanced sensing platforms for the detection of hydrogen sulfide. *TrAC Trends Anal. Chem.* **2018**, *105*, 263–281. [CrossRef]
71. Nagarkar, S.S.; Saha, T.; Desai, A.V.; Talukdar, P.; Ghosh, S.K. Metal-organic framework based highly selective fluorescence turn-on probe for hydrogen sulphide. *Sci. Rep.* **2014**, *4*, 7053. [CrossRef] [PubMed]
72. Nagarkar, S.S.; Desai, A.V.; Ghosh, S.K. A Nitro-Functionalized Metal–Organic Framework as a Reaction-Based Fluorescence Turn-On Probe for Rapid and Selective H_2S Detection. *Chem. Eur. J.* **2015**, *21*, 9994–9997. [CrossRef] [PubMed]
73. Zhang, X.; Zhang, J.; Hu, Q.; Cui, Y.; Yang, Y.; Qian, G. Postsynthetic modification of metal–organic framework for hydrogen sulfide detection. *Appl. Surf. Sci.* **2015**, *355*, 814–819. [CrossRef]
74. Buragohain, A.; Biswas, S. Cerium-based azide- and nitro-functionalized UiO-66 frameworks as turn-on fluorescent probes for the sensing of hydrogen sulphide. *CrystEngComm* **2016**, *18*, 4374–4381. [CrossRef]
75. Nandi, S.; Reinsch, H.; Banesh, S.; Stock, N.; Trivedi, V.; Biswas, S. Rapid and highly sensitive detection of extracellular and intracellular H_2S by an azide-functionalized Al(III)-based metal–organic framework. *Dalton Trans.* **2017**, *46*, 12856–12864. [CrossRef] [PubMed]
76. Dalapati, R.; Balaji, S.N.; Trivedi, V.; Khamari, L.; Biswas, S. A dinitro-functionalized Zr(IV)-based metal-organic framework as colorimetric and fluorogenic probe for highly selective detection of hydrogen sulphide. *Sens. Actuators B Chem.* **2017**, *245*, 1039–1049. [CrossRef]
77. Das, A.; Banesh, S.; Trivedi, V.; Biswas, S. Extraordinary sensitivity for H_2S and Fe(III) sensing in aqueous medium by Al-MIL-53-N_3 metal–organic framework: In vitro and in vivo applications of H_2S sensing. *Dalton Trans.* **2018**, *47*, 2690–2700. [CrossRef] [PubMed]
78. Nandi, S.; Banesh, S.; Trivedi, V.; Biswas, S. A dinitro-functionalized metal–organic framework featuring visual and fluorogenic sensing of H_2S in living cells, human blood plasma and environmental samples. *Analyst* **2018**, *143*, 1482–1491. [CrossRef]
79. Legrand, A.; Pastushenko, A.; Lysenko, V.; Geloen, A.; Quadrelli, E.A.; Canivet, J.; Farrusseng, D. Enhanced Ligand-Based Luminescence in Metal–Organic Framework Sensor. *ChemNanoMat* **2016**, *2*, 866–872. [CrossRef]
80. Zhang, X.; Zhang, Q.; Yue, D.; Zhang, J.; Wang, J.; Li, B.; Yang, Y.; Cui, Y.; Qian, G. Flexible Metal–Organic Framework-Based Mixed-Matrix Membranes: A New Platform for H_2S Sensors. *Small* **2018**, *14*, 1801563. [CrossRef]
81. Ma, Y.; Su, H.; Kuang, X.; Li, X.; Zhang, T.; Tang, B. Heterogeneous Nano Metal–Organic Framework Fluorescence Probe for Highly Selective and Sensitive Detection of Hydrogen Sulfide in Living Cells. *Anal. Chem.* **2014**, *86*, 11459–11463. [CrossRef]
82. Ma, Y.; Zhang, C.; Yang, P.; Li, X.; Tong, L.; Huang, F.; Yue, J.; Tang, B. A CuO-functionalized NMOF probe with a tunable excitation wavelength for selective detection and imaging of H_2S in living cells. *Nanoscale* **2018**, *10*, 15793–15798. [CrossRef]
83. Zhang, X.; Hu, Q.; Xia, T.; Zhang, J.; Yang, Y.; Cui, Y.; Chen, B.; Qian, G. Turn-on and Ratiometric Luminescent Sensing of Hydrogen Sulfide Based on Metal–Organic Frameworks. *ACS Appl. Mater. Interfaces* **2016**, *8*, 32259–32265. [CrossRef]

84. Zhang, X.; Fang, L.; Jiang, K.; He, H.; Yang, Y.; Cui, Y.; Li, B.; Qian, G. Nanoscale fluorescent metal–organic framework composites as a logic platform for potential diagnosis of asthma. *Biosens. Bioelectron.* **2019**, *130*, 65–72. [CrossRef]
85. Zheng, X.; Fan, R.; Song, Y.; Wang, A.; Xing, K.; Du, X.; Wang, P.; Yang, Y. A highly sensitive turn-on ratiometric luminescent probe based on postsynthetic modification of Tb^{3+}@Cu-MOF for H_2S detection. *J. Mater. Chem. C* **2017**, *5*, 9943–9951. [CrossRef]
86. Li, Y.; Zhang, X.; Zhang, L.; Jiang, K.; Cui, Y.; Yang, Y.; Qian, G. A nanoscale Zr-based fluorescent metal-organic framework for selective and sensitive detection of hydrogen sulfide. *J. Solid State Chem.* **2017**, *255*, 97–101. [CrossRef]
87. Cao, Y.-Y.; Guo, X.-F.; Wang, H. High sensitive luminescence metal-organic framework sensor for hydrogen sulfide in aqueous solution: A trial of novel turn-on mechanism. *Sens. Actuators B Chem.* **2017**, *243*, 8–13. [CrossRef]
88. Reddie, K.G.; Carroll, K.S. Expanding the functional diversity of proteins through cysteine oxidation. *Curr. Opin. Chem. Biol.* **2008**, *12*, 746–754. [CrossRef]
89. Dudev, T.; Lim, C. Metal Binding Affinity and Selectivity in Metalloproteins: Insights from Computational Studies. *Annu. Rev. Biophys.* **2008**, *37*, 97–116. [CrossRef]
90. Paulsen, C.E.; Carroll, K.S. Cysteine-Mediated Redox Signaling: Chemistry, Biology, and Tools for Discovery. *Chem. Rev.* **2013**, *113*, 4633–4679. [CrossRef]
91. Lieberman, M.W.; Wiseman, A.L.; Shi, Z.Z.; Carter, B.Z.; Barrios, R.; Ou, C.N.; Chévez-Barrios, P.; Wang, Y.; Habib, G.M.; Goodman, J.C.; et al. Growth retardation and cysteine deficiency in gamma-glutamyl transpeptidase-deficient mice. *Proc. Natl. Acad. Sci. USA* **1996**, *93*, 7923–7926. [CrossRef]
92. Wang, S.Q.; Shen, S.L.; Zhang, Y.R.; Dai, X.; Zhao, B.X. Recent Progress in Fluorescent Probes for the Detection of Biothiols. *Chin. J. Org. Chem.* **2014**, *34*, 1717–1729. [CrossRef]
93. Niu, L.-Y.; Chen, Y.-Z.; Zheng, H.-R.; Wu, L.-Z.; Tung, C.-H.; Yang, Q.-Z. Design strategies of fluorescent probes for selective detection among biothiols. *Chem. Soc. Rev.* **2015**, *44*, 6143–6160. [CrossRef]
94. Ding, S.; Liu, M.; Hong, Y. Biothiol-specific fluorescent probes with aggregation-induced emission characteristics. *Sci. China Chem.* **2018**, *61*, 882–891. [CrossRef]
95. Yin, C.-X.; Xiong, K.-M.; Huo, F.-J.; Salamanca, J.C.; Strongin, R.M. Fluorescent Probes with Multiple Binding Sites for the Discrimination of Cys, Hcy, and GSH. *Angew. Chem. Int. Ed.* **2017**, *56*, 13188–13198. [CrossRef]
96. Chen, X.; Zhou, Y.; Peng, X.; Yoon, J. Fluorescent and colorimetric probes for detection of thiols. *Chem. Soc. Rev.* **2010**, *39*, 2120–2135. [CrossRef]
97. Ren, X.; Tian, H.; Yang, L.; He, L.; Geng, Y.; Liu, X.; Song, X. Fluorescent probe for simultaneous discrimination of Cys/Hcy and GSH in pure aqueous media with a fast response under a single-wavelength excitation. *Sens. Actuators B Chem.* **2018**, *273*, 1170–1178. [CrossRef]
98. Yang, L.; Xiong, H.; Su, Y.; Tian, H.; Liu, X.; Song, X. A red-emitting water-soluble fluorescent probe for biothiol detection with a large Stokes shift. *Chin. Chem. Lett.* **2019**, *30*, 563–565. [CrossRef]
99. Sharma, S.; Ghosh, S.K. Metal–Organic Framework-Based Selective Sensing of Biothiols via Chemidosimetric Approach in Water. *ACS Omega* **2018**, *3*, 254–258. [CrossRef]
100. Wang, J.; Liu, Y.; Jiang, M.; Li, Y.; Xia, L.; Wu, P. Aldehyde-functionalized metal–organic frameworks for selective sensing of homocysteine over Cys, GSH and other natural amino acids. *Chem. Commun.* **2018**, *54*, 1004–1007. [CrossRef]
101. Gui, B.; Meng, Y.; Xie, Y.; Tian, J.; Yu, G.; Zeng, W.; Zhang, G.; Gong, S.; Yang, C.; Zhang, D.; et al. Tuning the Photoinduced Electron Transfer in a Zr-MOF: Toward Solid-State Fluorescent Molecular Switch and Turn-On Sensor. *Adv. Mater.* **2018**, *30*, 1802329. [CrossRef]
102. Zhao, X.; Zhang, Y.; Han, J.; Jing, H.; Gao, Z.; Huang, H.; Wang, Y.; Zhong, C. Design of "turn-on" fluorescence sensor for L-Cysteine based on the instability of metal-organic frameworks. *Microporous Mesoporous Mater.* **2018**, *268*, 88–92. [CrossRef]
103. Sen, A.; Desai, A.V.; Samanta, P.; Dutta, S.; Let, S.; Ghosh, S.K. Post-synthetically modified metal–organic framework as a scaffold for selective bisulphite recognition in water. *Polyhedron* **2018**, *156*, 1–5. [CrossRef]
104. Zhang, J.; Xia, T.; Zhao, D.; Cui, Y.; Yang, Y.; Qian, G. In situ secondary growth of Eu(III)-organic framework film for fluorescence sensing of sulfur dioxide. *Sens. Actuators B Chem.* **2018**, *260*, 63–69. [CrossRef]
105. Fang, F.C. Antimicrobial reactive oxygen and nitrogen species: Concepts and controversies. *Nat. Rev. Microbiol.* **2004**, *2*, 820–832. [CrossRef]

106. Li, H.; Cao, Z.; Moore, D.R.; Jackson, P.L.; Barnes, S.; Lambeth, J.D.; Thannickal, V.J.; Cheng, G. Microbicidal Activity of Vascular Peroxidase 1 in Human Plasma via Generation of Hypochlorous Acid. *Infect. Immun.* **2012**, *80*, 2528–2537. [CrossRef]
107. Bhattacharyya, A.; Chattopadhyay, R.; Mitra, S.; Crowe, S.E. Oxidative Stress: An Essential Factor in the Pathogenesis of Gastrointestinal Mucosal Diseases. *Physiol. Rev.* **2014**, *94*, 329–354. [CrossRef]
108. Soto, N.O.; Horstkotte, B.; March, J.G.; de Alba, P.L.L.; Martínez, L.L.; Martín, V.C. An environmental friendly method for the automatic determination of hypochlorite in commercial products using multisyringe flow injection analysis. *Anal. Chim. Acta* **2008**, *611*, 182–186. [CrossRef]
109. Ordeig, O.; Mas, R.; Gonzalo, J.; Del Campo, F.J.; Muñoz, F.J.; de Haro, C. Continuous Detection of Hypochlorous Acid/Hypochlorite for Water Quality Monitoring and Control. *Electroanalysis* **2005**, *17*, 1641–1648. [CrossRef]
110. Zhang, Y.-R.; Liu, Y.; Feng, X.; Zhao, B.-X. Recent progress in the development of fluorescent probes for the detection of hypochlorous acid. *Sens. Actuators B Chem.* **2017**, *240*, 18–36. [CrossRef]
111. Duan, Q.; Jia, P.; Zhuang, Z.; Liu, C.; Zhang, X.; Wang, Z.; Sheng, W.; Li, Z.; Zhu, H.; Zhu, B.; et al. Rational Design of a Hepatoma-Specific Fluorescent Probe for HOCl and Its Bioimaging Applications in Living HepG2 Cells. *Anal. Chem.* **2019**, *91*, 2163–2168. [CrossRef] [PubMed]
112. Wu, L.; Wu, I.C.; DuFort, C.C.; Carlson, M.A.; Wu, X.; Chen, L.; Kuo, C.-T.; Qin, Y.; Yu, J.; Hingorani, S.R.; et al. Photostable Ratiometric Pdot Probe for in Vitro and in Vivo Imaging of Hypochlorous Acid. *J. Am. Chem. Soc.* **2017**, *139*, 6911–6918. [CrossRef] [PubMed]
113. Nguyen, K.H.; Hao, Y.; Zeng, K.; Fan, S.; Li, F.; Yuan, S.; Ding, X.; Xu, M.; Liu, Y.-N. A benzothiazole-based fluorescent probe for hypochlorous acid detection and imaging in living cells. *Spectrochim. Acta A* **2018**, *199*, 189–193. [CrossRef] [PubMed]
114. Liang, S.; Kuang, Y.; Ma, F.; Chen, S.; Long, Y. A sensitive spectrofluorometric method for detection of berberine hydrochloride using Ag nanoclusters directed by natural fish sperm DNA. *Biosens. Bioelectron.* **2016**, *85*, 758–763. [CrossRef] [PubMed]
115. Zhang, P.; Wang, H.; Hong, Y.; Yu, M.; Zeng, R.; Long, Y.; Chen, J. Selective visualization of endogenous hypochlorous acid in zebrafish during lipopolysaccharide-induced acute liver injury using a polymer micelles-based ratiometric fluorescent probe. *Biosens. Bioelectron.* **2018**, *99*, 318–324. [CrossRef] [PubMed]
116. Zhang, P.; Wang, H.; Zhang, D.; Zeng, X.; Zeng, R.; Xiao, L.; Tao, H.; Long, Y.; Yi, P.; Chen, J. Two-photon fluorescent probe for lysosome-targetable hypochlorous acid detection within living cells. *Sens. Actuators B Chem.* **2018**, *255*, 2223–2231. [CrossRef]
117. Xue, M.; Wang, H.; Chen, J.; Ren, J.; Chen, S.; Yang, H.; Zeng, R.; Long, Y.; Zhang, P. Ratiometric fluorescent sensing of endogenous hypochlorous acid in lysosomes using AIE-based polymeric nanoprobe. *Sens. Actuators B Chem.* **2019**, *282*, 1–8. [CrossRef]
118. Zhou, Z.; Li, X.; Tang, Y.; Zhang, C.C.; Fu, H.; Wu, N.; Ma, L.; Gao, J.; Wang, Q. Oxidative deoximation reaction induced recognition of hypochlorite based on a new fluorescent lanthanide-organic framework. *Chem. Eng. J.* **2018**, *351*, 364–370. [CrossRef]
119. Ye, Y.; Zhao, L.; Hu, S.; Liang, A.; Li, Y.; Zhuang, Q.; Tao, G.; Gu, J. Specific detection of hypochlorite based on the size-selective effect of luminophore integrated MOF-801 synthesized by a one-pot strategy. *Dalton Trans.* **2019**, *48*, 2617–2625. [CrossRef]
120. Cai, K.; Zeng, M.; Wang, L.; Song, Y.; Chen, L. Ratiometric Fluorescent Detection of ClO^- Based on Dual-Emission F1-Rubpy@Nanoscale Metal-Organic Frameworks. *ChemistrySelect* **2019**, *4*, 2649–2655. [CrossRef]
121. Yue, D.; Zhao, D.; Zhang, J.; Zhang, L.; Jiang, K.; Zhang, X.; Cui, Y.; Yang, Y.; Chen, B.; Qian, G. A luminescent cerium metal–organic framework for the turn-on sensing of ascorbic acid. *Chem. Commun.* **2017**, *53*, 11221–11224. [CrossRef] [PubMed]
122. Yue, D.; Huang, Y.; Zhang, L.; Jiang, K.; Zhang, X.; Cui, Y.; Yu, Y.; Qian, G. Ratiometric luminescence sensing based on a mixed Ce/Eu metal–organic framework. *J. Mater. Chem. C* **2018**, *6*, 2054–2059. [CrossRef]
123. Yue, D.; Huang, Y.; Zhang, J.; Zhang, X.; Cui, Y.; Yang, Y.; Qian, G. A Two-Dimensional Metal–Organic Framework as a Fluorescent Probe for Ascorbic Acid Sensing. *Eur. J. Inorg. Chem.* **2018**, *2018*, 173–177. [CrossRef]
124. Wu, S.; Lin, Y.; Liu, J.; Shi, W.; Yang, G.; Cheng, P. Rapid Detection of the Biomarkers for Carcinoid Tumors by a Water Stable Luminescent Lanthanide Metal–Organic Framework Sensor. *Adv. Funct. Mater.* **2018**, *28*, 1707169. [CrossRef]

125. Chan, J.; Dodani, S.C.; Chang, C.J. Reaction-based small-molecule fluorescent probes for chemoselective bioimaging. *Nat. Chem.* **2012**, *4*, 973. [CrossRef] [PubMed]
126. Sk, M.; Banesh, S.; Trivedi, V.; Biswas, S. Selective and Sensitive Sensing of Hydrogen Peroxide by a Boronic Acid Functionalized Metal–Organic Framework and Its Application in Live-Cell Imaging. *Inorg. Chem.* **2018**, *57*, 14574–14581. [CrossRef] [PubMed]
127. Kotecha, P.V.; Patel, S.V.; Bhalani, K.D.; Shah, D.; Shah, V.S.; Mehta, K.G. Prevalence of dental fluorosis & dental caries in association with high levels of drinking water fluoride content in a district of Gujarat, India. *Indian J. Med. Res.* **2012**, *135*, 873–877.
128. Chirani, R.A.; Foray, H. Dental fluorosis: Etiological diagnosis. *Arch. Pediatr.* **2005**, *12*, 284–287. [CrossRef]
129. Souza, D.C.C.; Maltz, M.; Hashizume, L.N. Fluoride retention in saliva and in dental biofilm after different home-use fluoride treatments. *Braz. Oral Res.* **2014**, *28*, 255–259. [CrossRef]
130. Dhillon, A.; Nair, M.; Kumar, D. Analytical methods for determination and sensing of fluoride in biotic and abiotic sources: A review. *Anal. Methods* **2016**, *8*, 5338–5352. [CrossRef]
131. Wu, S.; Han, T.; Guo, J.; Cheng, Y. Poly(3-aminophenylboronic acid)-reduced graphene oxide nanocomposite modified electrode for ultrasensitive electrochemical detection of fluoride with a wide response range. *Sens. Actuators B Chem.* **2015**, *220*, 1305–1310. [CrossRef]
132. Snowden, T.S.; Anslyn, E.V. Anion recognition: Synthetic receptors for anions and their application in sensors. *Curr. Opin. Chem. Biol.* **1999**, *3*, 740–746. [CrossRef]
133. Michigami, Y.; Kuroda, Y.; Ueda, K.; Yamamoto, Y. Determination of urinary fluoride by ion chromatography. *Anal. Chim. Acta* **1993**, *274*, 299–302. [CrossRef]
134. Xu, X.R.; Li, H.B.; Gu, J.-D.; Paeng, K.J. Determination of Fluoride in Water by Reversed-Phase High-Performance Liquid Chromatography using F^--La^{3+}-Alizarin Complexone Ternary Complex. *Chromatographia* **2004**, *59*, 745–747. [CrossRef]
135. Han, J.; Zhang, J.; Gao, M.; Hao, H.; Xu, X. Recent advances in chromo-fluorogenic probes for fluoride detection. *Dyes Pigments* **2019**, *162*, 412–439. [CrossRef]
136. Zhou, Y.; Zhang, J.F.; Yoon, J. Fluorescence and Colorimetric Chemosensors for Fluoride-Ion Detection. *Chem. Rev.* **2014**, *114*, 5511–5571. [CrossRef]
137. Zhang, H.M.; Wu, Y.C.; You, J.Y.; Cao, L.; Ding, S.; Jiang, K.; Wang, Z.Y. New Progress in the Design, Synthesis and Application of Fluorescent Probes for Fluoride Ion Detection. *Chin. J. Org. Chem.* **2016**, *36*, 2559–2582. [CrossRef]
138. Wang, X.; Hu, R.; Li, S.Y. Design Strategy and Application of F^- Luminescent Probes. *Prog. Chem.* **2018**, *30*, 1364–1379.
139. Chen, B.; Wang, L.; Zapata, F.; Qian, G.; Lobkovsky, E.B. A Luminescent Microporous Metal–Organic Framework for the Recognition and Sensing of Anions. *J. Am. Chem. Soc.* **2008**, *130*, 6718–6719. [CrossRef]
140. Zheng, H.-Y.; Lian, X.; Qin, S.-J.; Yan, B. Novel "Turn-On" Fluorescent Probe for Highly Selectively Sensing Fluoride in Aqueous Solution Based on Tb^{3+}-Functionalized Metal–Organic Frameworks. *ACS Omega* **2018**, *3*, 12513–12519. [CrossRef]
141. Yang, Z.-R.; Wang, M.-M.; Wang, X.-S.; Yin, X.-B. Boric-Acid-Functional Lanthanide Metal–Organic Frameworks for Selective Ratiometric Fluorescence Detection of Fluoride Ions. *Anal. Chem.* **2017**, *89*, 1930–1936. [CrossRef] [PubMed]
142. Ebrahim, F.M.; Nguyen, T.N.; Shyshkanov, S.; Gładysiak, A.; Favre, P.; Zacharia, A.; Itskos, G.; Dyson, P.J.; Stylianou, K.C. Selective, Fast-Response, and Regenerable Metal–Organic Framework for Sampling Excess Fluoride Levels in Drinking Water. *J. Am. Chem. Soc.* **2019**, *141*, 3052–3058. [CrossRef] [PubMed]
143. Dorea, J.G.; Donangelo, C.M. Early (in uterus and infant) exposure to mercury and lead. *Clin. Nutr.* **2006**, *25*, 369–376. [CrossRef] [PubMed]
144. Harris, H.H.; Pickering, I.J.; George, G.N. The Chemical Form of Mercury in Fish. *Science* **2003**, *301*, 1203. [CrossRef] [PubMed]
145. Llobet, J.M.; Falcó, G.; Casas, C.; Teixidó, A.; Domingo, J.L. Concentrations of Arsenic, Cadmium, Mercury, and Lead in Common Foods and Estimated Daily Intake by Children, Adolescents, Adults, and Seniors of Catalonia, Spain. *J. Agric. Food. Chem.* **2003**, *51*, 838–842. [CrossRef] [PubMed]
146. Tchounwou, P.B.; Ayensu, W.K.; Ninashvili, N.; Sutton, D. Review: Environmental exposure to mercury and its toxicopathologic implications for public health. *Environ. Technol.* **2003**, *18*, 149–175. [CrossRef] [PubMed]
147. Harada, M. Minamata Disease: Methylmercury Poisoning in Japan Caused by Environmental Pollution. *Crit. Rev. Toxicol.* **1995**, *25*, 1–24. [CrossRef] [PubMed]

148. Chen, S.; Kuang, Y.; Zhang, P.; Huang, Y.; Wen, A.; Zeng, X.; Feng, R.; Nie, H.; Jiang, X.; Long, Y. A dual-functional spectroscopic probe for simultaneous monitoring Cu^{2+} and Hg^{2+} ions by two different sensing nature based on novel fluorescent gold nanoclusters. *Sens. Actuators B Chem.* **2017**, *253*, 283–291. [CrossRef]
149. Hao, Y.; Xiong, D.; Wang, L.; Chen, W.; Zhou, B.; Liu, Y.-N. A reversible competition colorimetric assay for the detection of biothiols based on ruthenium-containing complex. *Talanta* **2013**, *115*, 253–257. [CrossRef] [PubMed]
150. Cui, Y.; Hao, Y.; Zhang, Y.; Liu, B.; Zhu, X.; Qu, P.; Li, D.; Xu, M. A water-soluble and retrievable ruthenium-based probe for colorimetric recognition of Hg(II) and Cys. *Spectrochim. Acta A* **2016**, *165*, 150–154. [CrossRef] [PubMed]
151. Suherman, A.L.; Tanner, E.E.L.; Compton, R.G. Recent developments in inorganic Hg^{2+} detection by voltammetry. *TrAC Trends Anal. Chem.* **2017**, *94*, 161–172. [CrossRef]
152. Mahato, P.; Saha, S.; Das, P.; Agarwalla, H.; Das, A. An overview of the recent developments on Hg^{2+} recognition. *RSC Adv.* **2014**, *4*, 36140–36174. [CrossRef]
153. Chen, S.; Tang, J.; Kuang, Y.; Fu, L.; Ma, F.; Yang, Y.; Chen, G.; Long, Y. Selective deposition of HgS at the corner sites of triangular silver nanoprism and its tunable LSPR for colorimetric Hg^{2+} detection. *Sens. Actuators B Chem.* **2015**, *221*, 1182–1187. [CrossRef]
154. Quang, D.T.; Kim, J.S. Fluoro- and Chromogenic Chemodosimeters for Heavy Metal Ion Detection in Solution and Biospecimens. *Chem. Rev.* **2010**, *110*, 6280–6301. [CrossRef] [PubMed]
155. Kim, H.N.; Ren, W.X.; Kim, J.S.; Yoon, J. Fluorescent and colorimetric sensors for detection of lead, cadmium, and mercury ions. *Chem. Soc. Rev.* **2012**, *41*, 3210–3244. [CrossRef] [PubMed]
156. Yang, Y.; Zhao, Q.; Feng, W.; Li, F. Luminescent Chemodosimeters for Bioimaging. *Chem. Rev.* **2013**, *113*, 192–270. [CrossRef] [PubMed]
157. Samanta, P.; Desai, A.V.; Sharma, S.; Chandra, P.; Ghosh, S.K. Selective Recognition of Hg^{2+} ion in Water by a Functionalized Metal–Organic Framework (MOF) Based Chemodosimeter. *Inorg. Chem.* **2018**, *57*, 2360–2364. [CrossRef] [PubMed]
158. Panda, M.; Robinson, N.C. Kinetics and mechanism for the binding of HCN to cytochrome c oxidase. *Biochemistry* **1995**, *34*, 10009–10018. [CrossRef]
159. Jiang, J.; Wang, X.; Zhou, W.; Gao, H.; Wu, J. Extraction of gold from alkaline cyanide solution by the tetradecyldimethylbenzylammonium chloride/tri-n-butyl phosphate/n-heptane system based on a microemulsion mechanism. *Phys. Chem. Chem. Phys.* **2002**, *4*, 4489–4494. [CrossRef]
160. Attar, A.; Cubillana-Aguilera, L.; Naranjo-Rodríguez, I.; de Cisneros, J.L.; Palacios-Santander, J.M.; Amine, A. Amperometric inhibition biosensors based on horseradish peroxidase and gold sononanoparticles immobilized onto different electrodes for cyanide measurements. *Bioelectrochemistry* **2015**, *101*, 84–91. [CrossRef]
161. Kang, H.-I.; Shin, H.-S. Derivatization Method of Free Cyanide Including Cyanogen Chloride for the Sensitive Analysis of Cyanide in Chlorinated Drinking Water by Liquid Chromatography-Tandem Mass Spectrometry. *Anal. Chem.* **2015**, *87*, 975–981. [CrossRef] [PubMed]
162. Xu, Z.; Chen, X.; Kim, H.N.; Yoon, J. Sensors for the optical detection of cyanide ion. *Chem. Soc. Rev.* **2010**, *39*, 127–137. [CrossRef] [PubMed]
163. Wang, F.; Wang, L.; Chen, X.; Yoon, J. Recent progress in the development of fluorometric and colorimetric chemosensors for detection of cyanide ions. *Chem. Soc. Rev.* **2014**, *43*, 4312–4324. [CrossRef] [PubMed]
164. Udhayakumari, D. Chromogenic and fluorogenic chemosensors for lethal cyanide ion. A comprehensive review of the year 2016. *Sens. Actuators B Chem.* **2018**, *259*, 1022–1057. [CrossRef]
165. Hao, Y.; Nguyen, K.H.; Zhang, Y.; Zhang, G.; Fan, S.; Li, F.; Guo, C.; Lu, Y.; Song, X.; Qu, P.; et al. A highly selective and ratiometric fluorescent probe for cyanide by rationally altering the susceptible H-atom. *Talanta* **2018**, *176*, 234–241. [CrossRef] [PubMed]
166. Karmakar, A.; Kumar, N.; Samanta, P.; Desai, A.V.; Ghosh, S.K. A Post-Synthetically Modified MOF for Selective and Sensitive Aqueous-Phase Detection of Highly Toxic Cyanide Ions. *Chem. Eur. J.* **2016**, *22*, 864–868. [CrossRef]